

The helicase Ded1p controls use of near-cognate translation initiation codons in 5' UTRs

Ulf-Peter Guenther^{1,8}, David E. Weinberg^{2,3,4,8}, Meghan M. Zubradt^{2,5,8}, Frank A. Tedeschii¹, Brittany N. Stawicki¹, Leah L. Zagore¹, Gloria A. Brar⁶, Donny D. Licatalosi¹, David P. Bartel^{3,4}, Jonathan S. Weissman^{2,5} & Eckhard Jankowsky^{1,7*}

The conserved and essential DEAD-box RNA helicase Ded1p from yeast and its mammalian orthologue DDX3 are critical for the initiation of translation¹. Mutations in DDX3 are linked to tumorigenesis^{2–4} and intellectual disability⁵, and the enzyme is targeted by a range of viruses⁶. How Ded1p and its orthologues engage RNAs during the initiation of translation is unknown. Here we show, by integrating transcriptome-wide analyses of translation, RNA structure and Ded1p–RNA binding, that the effects of Ded1p on the initiation of translation are connected to near-cognate initiation codons in 5' untranslated regions. Ded1p associates with the translation pre-initiation complex at the mRNA entry channel and repressing the activity of Ded1p leads to the accumulation of RNA structure in 5' untranslated regions, the initiation of translation from near-cognate start codons immediately upstream of these structures and decreased protein synthesis from the corresponding main open reading frames. The data reveal a program for the regulation of translation that links Ded1p, the activation of near-cognate start codons and mRNA structure. This program has a role in meiosis, in which a marked decrease in the levels of Ded1p is accompanied by the activation of the alternative translation initiation sites that are seen when the activity of Ded1p is repressed. Our observations indicate that Ded1p affects translation initiation by controlling the use of near-cognate initiation codons that are proximal to mRNA structure in 5' untranslated regions.

To systematically analyse how Ded1p influences translation initiation in cells, we first examined how a mutation in the enzyme altered the spectrum of ribosome footprints in cells⁷. We used the *ded1-95* mutation (*Ded1p*^{T408I}), which reduces the affinity of Ded1p for RNA, diminishes RNA unwinding and confers a temperature-sensitive growth defect to the budding yeast *Saccharomyces cerevisiae*⁸. The mutation does not affect pre-mRNA splicing or ribosome biogenesis⁹. We performed ribosome profiling on wild-type and *ded1-95* strains before and after a temperature shift from 30 °C to 37 °C for 5 min (Extended Data Fig. 1a–h). The short time was chosen to minimize any secondary effects on ribosome footprints arising from broader translation defects.

At 30 °C, wild-type and *ded1-95* strains showed virtually indistinguishable RNA expression and translation profiles (Extended Data Fig. 1i, j). After the temperature shift, translation broadly decreased in *ded1-95*, compared to the wild type (Extended Data Fig. 1k–n). These observations indicate that Ded1p promotes translation initiation for most mRNAs, consistent with previous findings^{10,11}. However, translation of a subset of mRNAs coding for proteins involved in gluconeogenesis, cell wall synthesis and transcripts encoding histones were less affected by Ded1p than other mRNAs (Extended Data Fig. 2a, b).

The fraction of ribosomes on 5' untranslated regions (UTRs) markedly increased upon temperature shift in *ded1-95*, compared to the wild type (Fig. 1a, Extended Data Fig. 3a). The majority of mRNAs showed

higher ribosome occupancy of the 5' UTR in the *ded1-95* strain, which correlated with lower translation efficiency of the main open reading frame (ORF) (Fig. 1b, Extended Data Fig. 3b). To examine the link

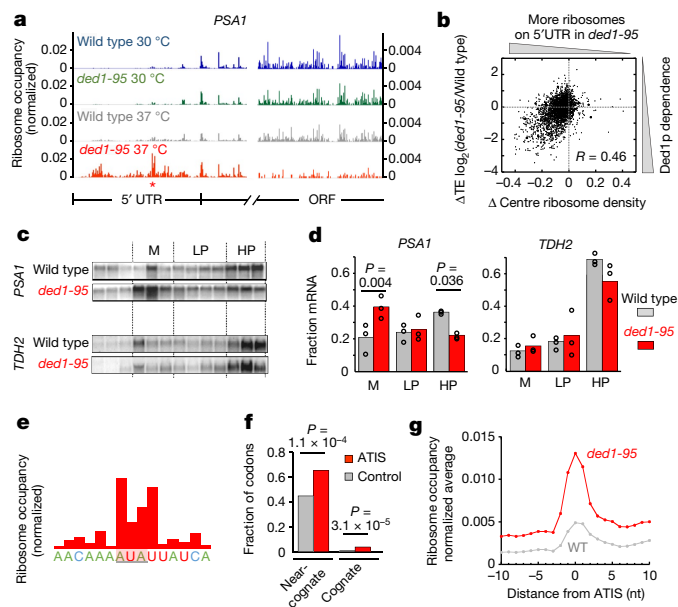


Fig. 1 | Defects in Ded1p activate alternative translation initiation sites. **a**, Ribosome profiling tracks of the 5' UTR of *PSA1* mRNA for wild-type *DED1* and *ded1-95*, before and 5 min after a temperature shift. Bars mark the ribosome P-site, the star an alternative translation initiation site. Similar results were obtained in two independent experiments for each dataset. **b**, Correlation between change in translational efficiency (ΔTE) and change in the centre of ribosome density of wild-type *DED1*, compared to *ded1-95* ($n = 2,837$, 5 min, 37 °C). R , Pearson's correlation coefficient. **c**, Representative RNA blots of *PSA1* ($\log_2 \Delta TE_{PSA1} = -2.1$) and *TDH2* ($\log_2 \Delta TE_{TDH2} = 0.7$) after polysome fractionation for wild-type *DED1* and *ded1-95*, 5 min after temperature shift. M, 80S monosomes; LP, light polysomes; HP, heavy polysomes. Similar results were obtained in three independent experiments. **d**, Quantification of *PSA1* and *TDH2* RNA blots. Bars indicate the fraction of the mRNA in monosomes (M), light polysomes (LP), and heavy polysomes (HP). P values from a two-tailed *t*-test. **e**, Representative ribosome profiling track for a segment in the 5' UTR of *PSA1* (indicated by the star in **a** in *ded1-95* (5 min, 37 °C)). The near-cognate initiation codon is highlighted. Similar results were obtained in two independent experiments. **f**, Fraction of near-cognate and cognate initiation codons at sites with marked ribosome accumulation (red bars, ATISs, $n = 396$), and at randomly chosen control positions (grey) in 5' UTRs in *ded1-95*. P values from a two-tailed *t*-test. **g**, Mean ribosome occupancy 10 nt 3' and 5' of high-confidence ATIS on 5' UTRs (moving average of ± 1 nt) for *ded1-95* (red) and wild-type *DED1* (5 min, 37 °C).

¹Center for RNA Science and Therapeutics, School of Medicine, Case Western Reserve University, Cleveland, OH, USA. ²Department of Cellular and Molecular Pharmacology, University of California, San Francisco, San Francisco, CA, USA. ³Howard Hughes Medical Institute Whitehead Institute for Biomedical Research, Cambridge, MA, USA. ⁴Department of Biology, Massachusetts Institute of Technology, Cambridge, MA, USA. ⁵Howard Hughes Medical Institute California Institute for Quantitative Biomedical Research, San Francisco, CA, USA. ⁶Department of Molecular and Cell Biology, University of California, Berkeley, CA, USA. ⁷Department of Physics, Case Western Reserve University, Cleveland, OH, USA. ⁸These authors contributed equally: Ulf-Peter Guenther, David E. Weinberg, Meghan M. Zubradt. *e-mail: exj13@case.edu

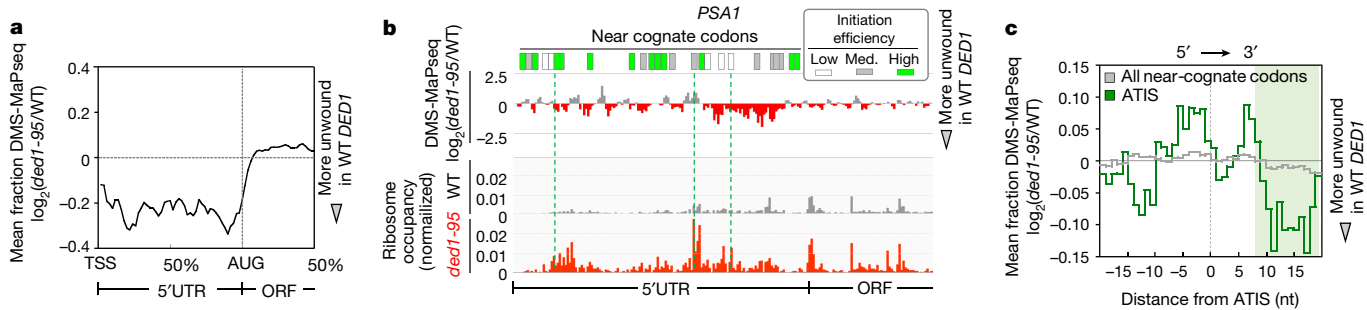


Fig. 2 | mRNA structure unwinding by Ded1p and ATIS activation.

a, Metagene profile of mRNA unwinding by Ded1p on 5' UTRs and the 5' moiety of ORFs (moving average of ± 1 nt). Similar results were obtained in two independent experiments. TSS, transcription start site; AUG, translation start site. b, Representative differential DMS mutational profiling with sequencing (DMS-MaPseq) track for the 5' UTR of the *PSA1* mRNA (upper track, mRNA regions unwound in wild-type *DED1* (WT) marked by red bars, the more negative the value, the stronger the unwinding). Similar results were obtained in two independent experiments. For comparison, ribosome profiling traces of the 5' UTR of *PSA1* mRNA for wild-type *DED1* and *ded1-95* are shown. Near-cognate

codons are colour-coded according to their initiation efficiency, as indicated. Green lines mark activated ATISs. c, Localization of unwound mRNA structure 3' of activated ATISs. Enrichment of differential DMS-MaPseq counts. Negative values indicate unwound mRNA regions in wild-type *DED1* within 20 nt of high-stringency ATISs ($n = 274$), compared to all other near-cognate codons ($n = 60,666$; excluding ATIS). The shaded area marks a significant difference in secondary RNA structure between the regions downstream of an ATIS and downstream of any near-cognate codon ($P = 0.00004$, two-tailed *t*-test). The dashed line marks the 5' nucleotide of the ATISs or the near-cognate codon.

between increased ribosome occupancy in the 5' UTR and diminished translation of the main ORF, we performed polysome fractionation with northern blot analysis of individual mRNAs. The *PSA1* mRNA—the translation efficiency of which is markedly affected by Ded1p—showed a distinct shift from polysomes to monosomes in *ded1-95* compared to the wild type, upon temperature shift but not at 30 °C (Fig. 1c, d, Extended Data Fig. 3c). *TDH2* mRNA, which is largely unaffected by Ded1p, did not show a comparable shift (Fig. 1c, d). Collectively, these observations suggest that increased ribosome occupancy on 5' UTRs correlates with binding of the mRNA to only a single ribosome. This notion is consistent with previous reports¹². Ribosome profiling on only the 80S monosome fraction upon temperature shift also showed more footprints on 5' UTRs in the *ded1-95* strain, compared to the wild type (Extended Data Fig. 3d), indicating that ribosome occupancy on 5' UTRs broadly correlates with the binding of mRNAs to single ribosomes.

A large number of sites on 5' UTRs with increased ribosome footprints in the *ded1-95* strain were enriched with near-cognate initiation codons (Fig. 1e–g), which differ from the canonical 5'-AUG-3' initiation codon by a single nucleotide and can create alternative translation initiation sites (ATISs)¹³. Increased ribosome occupancy on AUG codons in 5' UTRs was also seen in the *ded1-95* strain (Fig. 1f), but only a few of these sites exist in the yeast transcriptome, compared to nine different near-cognate initiation codons, which constitute roughly 14% of all codons¹⁴. Ribosomes can translate from the *ded1-95*-activated ATISs, as demonstrated by ribosome profiles on small ORFs that start at these ATISs and finish at the respective termination codons, by the lack of ribosome accumulation at ATISs when translation was not arrested and by the periodicity of ribosome footprints starting from ATISs (Extended Data Fig. 3e–l). Collectively, the data indicate that defective Ded1p leads to ATIS activation in 5' UTRs, which decreases polysome formation on the main ORFs and thereby overall protein production. We conclude that Ded1p function suppresses the use of ATISs.

Although ATIS activation in *ded1-95* was extensive, only a subset of all near-cognate initiation codons was used. We detected no preferred length or register of the corresponding small ORFs relative to the main ORFs. However, in the ATISs, near-cognate codons from which translation initiation is most efficient were over-represented, whereas near-cognate codons from which translation initiation is least efficient were underrepresented^{15,16} (Extended Data Fig. 4a). These observations show that ATIS activation is influenced by inherent codon preferences of the pre-initiation complex (PIC), although these preferences do not fully explain the ATIS activation pattern (Extended Data Fig. 4b–e).

To better understand this pattern, we examined whether remodelling of mRNA secondary structure by Ded1p is linked to ATIS activation. As

an RNA helicase, Ded1p has been implicated in RNA structure remodelling^{11,17}, but it is not known which mRNA structures Ded1p alters in cells. To delineate the cellular mRNA structures that are remodelled by Ded1p, we used dimethyl sulfate (DMS) probing *in vivo*¹⁸ and measured changes in mRNA structure in *ded1-95* and wild-type strains upon temperature shift (Extended Data Fig. 5a, b). Unwinding of mRNA structure by Ded1p was most pronounced in 5' UTRs, compared to other mRNA regions (Fig. 2a, Extended Data Fig. 5c). Notably, *ded1-95* activated ATISs were generally located 5' of unwound RNA regions (Fig. 2b, c). Even near-cognate codons for which translation initiation is least efficient were activated, if they were located 5' of mRNA structure (Fig. 2b). Our observations link the inability of *ded1-95* to resolve mRNA structure to ATIS activation, suggesting that Ded1p suppresses ATIS activation by unwinding mRNA structure.

To investigate how Ded1p physically accomplishes this function, we determined which cellular RNAs bound to wild-type Ded1p using a high-throughput cross-linking-based approach (cross-linking-aided RNA affinity precipitation with sequencing (XL-RAP-seq)) and the individual-nucleotide resolution cross-linking and immunoprecipitation (iCLIP) technique to map Ded1p-binding sites on these RNAs¹⁹ (Extended Data Fig. 6a–c). Ded1p cross-linked predominantly to mRNAs and ribosomal RNA (Extended Data Fig. 6b), especially to the 40S ribosomal subunit (Fig. 3a), which is part of the PIC that scans 5' UTRs²⁰. The most frequently cross-linked position maps to helix 16, located at the mRNA entry channel (Fig. 3a). Notable cross-linking was also observed at helix 26, which is located at the mRNA exit site, and in extension segment 6 (around nucleotide 720), which is located in the vicinity of the other cross-link sites on the solvent side of the 40S subunit (Fig. 3a). Ded1p binding to helices 16 and 26 is consistent with reported interactions between Ded1p and eIF3c and the eIF3b–eIF3g–eIF3i sub-complex, that binds near these sites^{21,22} (Extended Data Fig. 7a, b). Human DDX3X also binds to helix 16³.

Ded1p further cross-linked to virtually all expressed mRNAs, predominantly in 5' UTRs (Fig. 3b, c). This cross-linking pattern is consistent with the physical contact of Ded1p to the PIC. Aside from a modest preference for A and U, no sequence motifs could be identified in the mRNA cross-linking sites (Extended Data Fig. 7c). However, peaks of Ded1p cross-linking on 5' UTRs were frequently proximal to *ded1-95*-activated ATISs (Fig. 3c, d), and unwound mRNA structure was located 3' of Ded1p cross-linking sites (Fig. 3c, f).

Collectively, the data link Ded1p binding to mRNA, unwound mRNA structure, ATIS location and binding of Ded1p to the PIC. This link is illustrated by a segment of the *PSA1* mRNA as an example (Fig. 4a). Ded1p binding is most pronounced 5' of unwound RNA

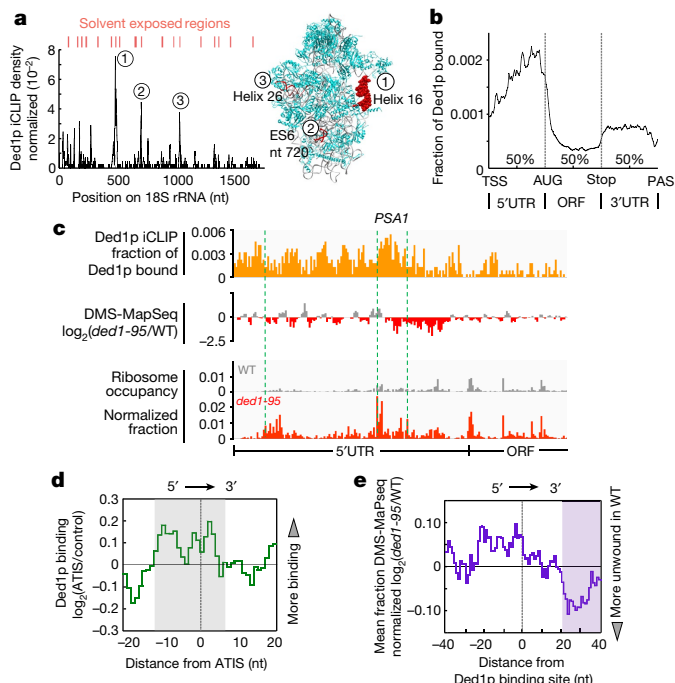


Fig. 3 | Ded1p cross-linking to the 40S ribosomal subunit and to mRNAs. **a**, Left, fraction of iCLIP reverse transcription stops on 18S rRNA. Moving average of ± 2 nt, values represent the average from two independent experiments. Numbers denote predominant cross-linking sites. Right, the position of the three predominant Ded1p cross-linking sites (red) in the crystal structure of the 40S ribosomal subunit³⁰. RNA, grey; ribosomal proteins, cyan; Ded1p cross-link sites, red. ES6, extension segment 6. **b**, Metagene profile of Ded1p association to mRNAs, calculated from two independent iCLIP experiments (moving average of ± 1 nt). Stop, translation stop site; PAS, polyadenylation site. **c**, Ded1p cross-linking to the 5' UTR of the *PSA1* mRNA. Top, fraction of reverse transcription stops per nucleotide, normalized to transcript length. For comparison, differential DMS-MapSeq (middle) and ribosome profiling (bottom) tracks of the 5' UTR of *PSA1* mRNA for wild-type *DED1* and *ded1-95* are shown (5 min, 37 °C). Similar results were obtained in two independent experiments. **d**, Enrichment of Ded1p cross-linking within 20 nt of ATISs ($n = 274$) normalized to the background distribution of Ded1p binding (moving average of ± 1 nt, reverse transcription stops normalized for each mRNA). The dashed line marks the ATIS position. The shaded area marks a significant difference in Ded1p binding between the regions in the vicinity of an ATIS and in the vicinity of a random position within the same 5' UTR ($P = 0.013$, two-tailed *t*-test). **e**, Enrichment of differential DMS-MapSeq counts (Fig. 2c) within 40 nt of Ded1p binding sites ($n = 178$, high-stringency ATIS) on 5' UTRs. The shaded area marks a significant difference in RNA structure between the regions downstream of a Ded1p binding site and downstream of a random position within the same 5' UTR ($P = 0.008$, two-tailed *t*-test).

structure, indicating that Ded1p does not exclusively contact mRNA structure, but also regions that are 5' of the structure. This finding is consistent with the notion that Ded1p functions in the context of the scanning PIC. The scanning process is slowed by RNA structure^{20,23}, and a slowed PIC conceivably permits Ded1p to survey the mRNA for structured regions that it then unwinds. Biochemical data show higher functional affinity of Ded1p for unstructured RNA, compared to structured RNA⁸, rationalizing the contacts of Ded1p to unpaired mRNA that is 5' of unwound mRNA structure, as the helicase travels in a 5' to 3' direction with the PIC.

Our data collectively indicate that failure of Ded1p to resolve mRNA structure leads to ATIS activation. To directly probe the link between mRNA unwinding and ATIS activation, we generated a *PSA1* mRNA with a mutation in an activated ATIS 5' of unwound RNA structure (Fig. 4b). The mutation markedly diminished the sensitivity to Ded1p-deficiency seen with the native *PSA1* mRNA (Fig. 4b, c). Alterations in

the RNA structure 3' of the ATIS also decreased sensitivity to Ded1p (Extended Data Fig. 8a, b). Identical observations were made for mutations in an ATIS and the corresponding RNA structure in the *ATP5* mRNA (Extended Data Fig. 8c–f). These results show that the effect of Ded1p on translation initiation depends not only on RNA unwinding, but also on proximal ATISs. Without a proximal ATIS, failure of Ded1p to unwind 5' UTR structures does not abrogate scanning of the PIC and subsequent translation of the main ORF (Extended Data Fig. 9). This finding challenges the notion that cellular 5' UTR structures alone are insurmountable hindrances for the scanning PIC.

Together, our results suggest the following function for Ded1p on 5' UTRs (Fig. 4d). The enzyme associates with the PIC in the vicinity of the mRNA entry site of the small ribosomal subunit (Fig. 3a). This site is in close proximity to eIF4G and eIF4A (Extended Data Fig. 7b), both of which bind Ded1p with high affinity and might therefore be important for recruitment and function of Ded1p on the PIC^{8,24,25}. The density of Ded1p cross-linking sites on 5' UTRs increases with distance from the 5' cap (Fig. 3b), suggesting gradual recruitment of Ded1p to the mRNA entry site during the scanning process. This notion is consistent with the reported increase of Ded1p function with greater distance from the 5' cap and with 5' UTR length¹¹. The mRNA binding pattern of Ded1p further suggests that Ded1p is targeted to its sites of action through association with the scanning PIC. This is an effective way to deploy the enzyme exactly at sites at which it is needed, even though these sites lack common sequence or defined structure signatures. If Ded1p is missing or defective, mRNA structure persists, the PIC stalls and either dissociates from the mRNA, continues slowed scanning through the structure, or undergoes subunit joining and translation initiation if a near-cognate codon is present (Fig. 4d). Ribosomes initiating on an ATIS block subsequent scanning ribosomes from reaching the canonical initiation site, thereby decreasing translation efficiency for the main ORF (Fig. 1b). Unless an ATIS marks an N-terminal extension of the main ORF, PICs initiating at an ATIS are likely to be deterred from translating the main ORF. PICs encountering 5' UTR structures without a proximal ATIS also interfere with scanning, but the kinetic pause introduced by PIC stalling, slowed scanning through the structure or a combination thereof is shorter than on an activated ATIS. Slowed PICs will eventually reach the main ORF (Extended Data Fig. 9), and therefore 5' UTR structure alone affects main ORF translation less in isolation than it does in combination with proximal ATISs. Our model for Ded1p function does not preclude additional roles of the enzyme before the PIC scanning process²⁵. However, the Ded1p function outlined above largely accounts for the observed Ded1p interactions with mRNA, and therefore, additional roles of Ded1p are probably restricted to transient Ded1p–mRNA interactions.

Finally, our data reveal a straightforward mechanism for activation of upstream ORFs. The mRNA structures in the 5' UTRs represent a large set of riboswitches that are sensitive to Ded1p. Active Ded1p turns the switches off, suppresses ATIS activation and allows efficient translation of the main ORF. Inactivation of the helicase by post-translational modifications¹, by metabolites such as AMP²⁶, by decreased Ded1p levels or by sequestration of Ded1p in RNP granules^{25,27} turns the switches on, activating the ATISs and thereby inhibiting translation from the corresponding main ORFs. Certain peptides that are translated from activated ATISs might also have direct biological functions²⁸, but the regulation described here appears to be independent of functional peptides.

This mechanism for activation of upstream ORFs is probably used in biological processes. This notion is supported by several lines of evidence. First, there is a marked increase in sequence conservation in the RNA regions around activated ATIS (Extended Data Fig. 10a). Second, the *ded1-95* activated ATIS in the *ALA1* transcript produces an N-terminal extension that targets Ala1p to the mitochondria²⁹ (Extended Data Fig. 10b). Third, during meiosis, ATIS activation¹⁵ occurs in a pattern that is highly similar to the ATIS activation pattern seen with *ded1-95* upon temperature shift (Fig. 4e, f, Extended Data Fig. 10c). Notably, we find reduced Ded1p levels during meiosis (Fig. 4g, Extended Data Fig. 10d). This link between Ded1p levels and

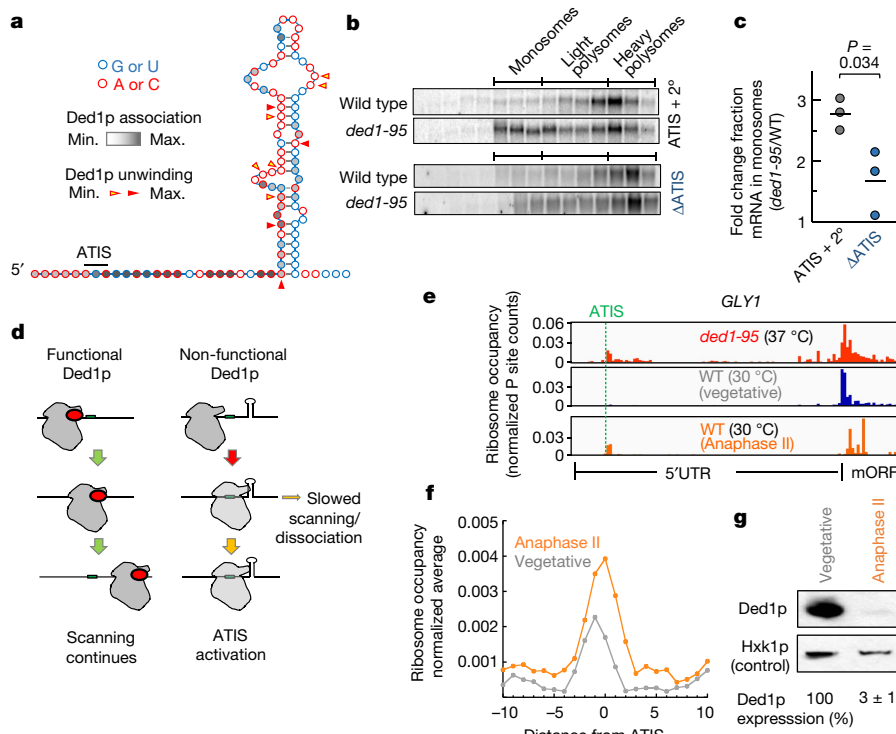


Fig. 4 | Ded1p function on 5' UTRs. **a**, DMS-MapSeq constrained secondary structure model of a fragment of the *PSA1* mRNA 5' UTR. The ATIS is marked by a line. Shading indicates Ded1p cross-linking (iCLIP). Triangles indicate unwinding (DMS-MapSeq) for each nucleotide (\log_2 ratio of normalized DMS-MapSeq counts of wild type/*ded1-95* in two categories). Yellow triangles, 0.35–0.7 (moderately unwound) and red triangles, >0.7 (strongly unwound). **b**, Representative RNA blots, after sucrose gradient centrifugation for wild-type *DED1* and *ded1-95*, (5 min, 37 °C) for constructs expressing *PSA1-FLAG* mRNA with wild-type 5' UTR (ATIS and secondary structure (Δ^2)) or with a mutated ATIS (Δ ATIS). Similar results were obtained in three independent experiments. **c**, Quantification of RNA blot experiments shown in **b**, indicating the fold change in the fraction of *PSA1* mRNA in monosomes in *ded1-95*, compared to the wild type upon temperature shift. Data are from three

independent biological replicates, lines mark the mean. *P* value from a two-tailed *t*-test. **d**, Schematic of Ded1p function on 5' UTRs. mRNA is depicted as a black line, mRNA structure as a hairpin, the PIC as a grey shape, Ded1p as a red oval, and the near-cognate codon as a green rectangle. **e**, Ribosome occupancy tracks (5 min, 37 °C) of *ded1-95* and wild-type *DED1* (vegetative control and anaphase II) for *GLY1* mRNA. ATISs are marked by dashed lines. Similar results were obtained in two (vegetative control) and four (anaphase II) independent experiments. mORF, main ORF. **f**, Mean ribosome occupancy 10 nt 3' and 5' of a high-confidence ATIS on 5' UTRs (moving average \pm 1nt) for wild-type *DED1* (vegetative control and anaphase II). **g**, Representative western blot of Ded1p and Hxk1p (loading control) in vegetative cells and cells in anaphase II. Numbers indicate the relative expression level of Ded1p from four independent experiments with s.d.

the activation of ATISs proximal to 5' UTR structures during meiosis suggests a role for the levels of Ded1p in this process. Collectively, our observations show that the regulatory program linking Ded1p to mRNA structure and ATIS activation is used in a physiological cellular process. The results indicate that intricate translation control and activation of upstream ORFs can be based on simple, ubiquitous elements: a helicase, mRNA structure and near-cognate initiation codons.

Online content

Any Methods, including any statements of data availability and Nature Research reporting summaries, along with any additional references and Source Data files, are available in the online version of the paper at <https://doi.org/10.1038/s41586-018-0258-0>.

Received: 30 January 2017; Accepted: 8 May 2018;

Published online 27 June 2018.

- Sharma, D. & Jankowsky, E. The Ded1/DDX3 subfamily of DEAD-box RNA helicases. *Crit. Rev. Biochem. Mol. Biol.* **49**, 343–360 (2014).
- Bol, G. M., Xie, M. & Raman, V. DDX3, a potential target for cancer treatment. *Mol. Cancer* **14**, 188 (2015).
- Oh, S. et al. Medulloblastoma-associated DDX3 variant selectively alters the translational response to stress. *Oncotarget* **7**, 28169–28182 (2016).
- Pugh, T. J. et al. Medulloblastoma exome sequencing uncovers subtype-specific somatic mutations. *Nature* **488**, 106–110 (2012).
- Snijders Blok, L. et al. Mutations in DDX3X are a common cause of unexplained intellectual disability with gender-specific effects on Wnt signaling. *Am. J. Hum. Genet.* **97**, 343–352 (2015).
- Valiente-Echeverría, F., Hermoso, M. A. & Soto-Rifo, R. RNA helicase DDX3: at the crossroad of viral replication and antiviral immunity. *Rev. Med. Virol.* **25**, 286–299 (2015).
- Ingolia, N. T., Brar, G. A., Rouskin, S., McGeechey, A. M. & Weissman, J. S. The ribosome profiling strategy for monitoring translation in vivo by deep sequencing of ribosome-protected mRNA fragments. *Nat. Protocols* **7**, 1534–1550 (2012).
- Putnam, A. A. et al. Division of labor in an oligomer of the DEAD-box RNA helicase Ded1p. *Mol. Cell* **59**, 541–552 (2015).
- Burckin, T. et al. Exploring functional relationships between components of the gene expression machinery. *Nat. Struct. Mol. Biol.* **12**, 175–182 (2005).
- Chuang, R. Y., Weaver, P. L., Liu, Z. & Chang, T. H. Requirement of the DEAD-box protein Ded1p for messenger RNA translation. *Science* **275**, 1468–1471 (1997).
- Sen, N. D., Zhou, F., Ingolia, N. T. & Hinnebusch, A. G. Genome-wide analysis of translational efficiency reveals distinct but overlapping functions of yeast DEAD-box RNA helicases Ded1 and eIF4A. *Genome Res.* **25**, 1196–1205 (2015).
- Heyer, E. E. & Moore, M. J. Redefining the translational status of 80S monosomes. *Cell* **164**, 757–769 (2016).
- Hinnebusch, A. G., Ivanov, I. P. & Sonenberg, N. Translational control by 5'-untranslated regions of eukaryotic mRNAs. *Science* **352**, 1413–1416 (2016).
- Ingolia, N. T., Ghaemmaghami, S., Newman, J. R. & Weissman, J. S. Genome-wide analysis in vivo of translation with nucleotide resolution using ribosome profiling. *Science* **324**, 218–223 (2009).
- Brar, G. A. et al. High-resolution view of the yeast meiotic program revealed by ribosome profiling. *Science* **335**, 552–557 (2012).
- Kolitz, S. E., Takacs, J. E. & Lorsch, J. R. Kinetic and thermodynamic analysis of the role of start codon/anticodon base pairing during eukaryotic translation initiation. *RNA* **15**, 138–152 (2008).
- Berthelot, K., Muldoon, M., Rajkowitsch, L., Hughes, J. & McCarthy, J. E. Dynamics and processivity of 40S ribosome scanning on mRNA in yeast. *Mol. Microbiol.* **51**, 987–1001 (2004).

18. Zubradt, M. et al. DMS-MaPseq for genome-wide or targeted RNA structure probing *in vivo*. *Nat. Methods* **14**, 75–82 (2017).
19. Huppertz, I. et al. iCLIP: protein-RNA interactions at nucleotide resolution. *Methods* **65**, 274–287 (2014).
20. Hinnebusch, A. G. The scanning mechanism of eukaryotic translation initiation. *Annu. Rev. Biochem.* **83**, 779–812 (2014).
21. Gavin, A. C. et al. Proteome survey reveals modularity of the yeast cell machinery. *Nature* **440**, 631–636 (2006).
22. Krogan, N. J. et al. High-definition macromolecular composition of yeast RNA-processing complexes. *Mol. Cell* **13**, 225–239 (2004).
23. Kozak, M. Downstream secondary structure facilitates recognition of initiator codons by eukaryotic ribosomes. *Proc. Natl Acad. Sci. USA* **87**, 8301–8305 (1990).
24. Gao, Z. et al. Coupling between the DEAD-box RNA helicases Ded1p and eIF4A. *eLife* **5**, e16408 (2016).
25. Hilliker, A., Gao, Z., Jankowsky, E. & Parker, R. The DEAD-box protein Ded1 modulates translation by the formation and resolution of an eIF4F-mRNA complex. *Mol. Cell* **43**, 962–972 (2011).
26. Putnam, A. A. & Jankowsky, E. AMP sensing by DEAD-box RNA helicases. *J. Mol. Biol.* **425**, 3839–3845 (2013).
27. Jain, S. et al. ATPase-modulated stress granules contain a diverse proteome and substructure. *Cell* **164**, 487–498 (2016).
28. Andrews, S. J. & Rothnagel, J. A. Emerging evidence for functional peptides encoded by short open reading frames. *Nat. Rev. Genet.* **15**, 193–204 (2014).
29. Tang, H. L. et al. Translation of a yeast mitochondrial tRNA synthetase initiated at redundant non-AUG codons. *J. Biol. Chem.* **279**, 49656–49663 (2004).
30. Aylett, C. H., Boehringer, D., Erzberger, J. P., Schaefer, T. & Ban, N. Structure of a yeast 40S-eIF1-eIF1A-eIF3-eIF3j initiation complex. *Nat. Struct. Mol. Biol.* **22**, 269–271 (2015).

Acknowledgements This study was supported by the National Institutes of Health (NIH) (GM118088 to E.J., GM107331 to D.D.L.) and by a postdoctoral

fellowship from the German Research Council (GU 1146/1-1 to U.-P.G.). D.P.B. and J.S.W. are investigators of the Howard Hughes Medical Institute. We thank M. Adams for help with the initial data analysis; N. Al-Huseini and J. Collier for discussion and materials; A. Tambe, M. Hannigan, and R. Backofen for advice on bioinformatic data analysis; B. Klaus for critical advice on statistical analysis and M. Hentze for discussion.

Reviewer information Nature thanks P. Todd and the other anonymous reviewer(s) for their contribution to the peer review of this work.

Author contributions U.-P.G.: conceptualization, material generation, ribosome profiling, XL-RAP-seq, iCLIP, molecular biology techniques, bioinformatic analysis, statistical analysis and manuscript writing; D.E.W.: conceptualization and iCLIP; M.M.Z.: conceptualization, DMS-MaPseq and bioinformatic analysis; F.A.T.: iCLIP, bioinformatic analysis, western blots; B.N.S.: material generation and northern blots; L.L.Z. and D.D.L.: iCLIP; G.A.B.: material generation and meiosis strains; D.P.B.: conceptualization and study supervision; J.S.W.: conceptualization and study supervision; E.J.: conceptualization, study supervision and manuscript writing. All authors commented on and edited the manuscript.

Competing interests The authors declare no competing interests.

Additional information

Extended data is available for this paper at <https://doi.org/10.1038/s41586-018-0258-0>.

Supplementary information is available for this paper at <https://doi.org/10.1038/s41586-018-0258-0>.

Reprints and permissions information is available at <http://www.nature.com/reprints>.

Correspondence and requests for materials should be addressed to E.J.

Publisher's note: Springer Nature remains neutral with regard to jurisdictional claims in published maps and institutional affiliations.

METHODS

No statistical methods were used to predetermine sample size. The experiments were not randomized and the investigators were not blinded to allocation during experiments and outcome assessment.

Yeast strains, plasmids and oligonucleotides. Yeast strains used in this study are listed in Supplementary Table 1. Strains were grown at 30 °C unless stated otherwise. Primers, northern blot probes and other DNA oligonucleotides are listed in Supplementary Table 2, RNA oligonucleotides are listed in Supplementary Table 3, and DNA plasmids are listed in Supplementary Table 4.

Generation of a yeast strain expressing Ded1p–HTB. Construction of plasmid pEJ21 containing the N-terminally haemagglutinin (HA)-tagged Ded1p has previously been described²⁴. pEJ21 was then used to generate the plasmid pEJ5. The HA tag was replaced by a sequence containing a HpaI and a SphI site (amplification with primers X1 and X2), generating pEJ1. The His₆-TEV-Biotin (HTB) tag was amplified from pFA6-HTB-kanMX6 plasmid (gift from P. Kaiser) with primers X3 and X4. The resulting PCR product was cloned into pEJ1 via its HpaI and SphI sites yielding pEJ2. A second His₆ tag was introduced by site-directed mutagenesis with primers X5 and X6 generating pEJ3. The C-terminal His₆-TEV-Biotin-His₆ (HTB) tag was introduced into pEJ4²⁴ by amplification of pEJ3 with primers X8 and X9 and subcloning with PflMI and SpeI into pEJ4, yielding pEJ5. pEJ5 was linearized and used to transform BY4741 by standard lithium acetate transformation yielding yeast strain yEJ2.

Generation of a yeast strain expressing Ded1p–His₆–FLAG₃. Yeast strain yDPB740, containing a C-terminal His₆–FLAG₃ tag on the endogenous *DED1* allele, was generated from BY4742 using standard methods. In brief, a homologous recombination template was designed comprising the 40 nucleotides upstream and downstream of the *DED1* stop codon flanking the His₆FLAG₃ tag (with stop codon) and kanMX6 drug resistance cassette. This template was generated by amplifying from pFA6a–6×His–3×FLAG–kanMX6 plasmid with primers DW1 and DW2. PCR product was used to transform BY4742 by standard lithium acetate transformation yielding yeast strain yDPB740.

Generation of a yeast strain expressing wild-type, ΔATIS and secondary structure mutants of *PSA1* and *ATP5* mRNAs. FLAG-tagged *PSA1* and *ATP5* strains were generated from the respective cDNAs using standard methods as described above (pEJ14, pEJ15 and pEJ18, pEJ19, respectively). The FLAG-tag was appended at the 3' terminus of the *PSA1* and *ATP5* ORF, respectively. For *PSA1*, mutations in the ATIS in the 5' UTR (*PSA1*–ΔATIS, pEJ16, Fig. 4b, c) contained the following changes: (c.-58A>C (c.-58 indicates the 58th nucleotide 3' of the A of the AUG), c.-56A>C, c.-52T>A). Mutations in the 5' UTR mRNA structure (*PSA1*–Δ², pEJ17, Extended Data Fig. 8a, b), contained the following changes: (c.-39_–38AG>TC, c.-36_–35TA>AT, c.-32A>T, c.-24_–22AAA>TCT, c.-19_–18AA>CT). For *ATP5*, mutations in the ATIS in the 5' UTR (*ATP5*–ΔATIS, pEJ20, Extended Data Fig. 8e, f) contained the following changes: (c.-126A>C, c.-120_–119TT>CC, c.-109A>C). Mutations in the 5' UTR mRNA structure (*ATP5*–Δ², pEJ22, Extended Data Fig. 8e, f), contained the following changes: (c.-102C>A, c.-99C>A, c.-96G>A, c.-83G>A, c.-81C>A, c.-76G>A, c.-74G>A).

Polyosome analysis. Polyosome analysis using 20U (A₂₆₀) lysate was performed as described³¹, with a lower final concentration of cycloheximide (50 µg ml⁻¹). In brief, after centrifugation through a 15–45% (w/v) sucrose gradient, sixteen fractions were collected at a pump speed of *S* = 0.9 ml min⁻¹. RNA in each fraction was precipitated by adding two volumes of ice-cold ethanol and incubating overnight at –80 °C. RNA was extracted with phenol–chloroform according to standard protocols. Samples were applied to a 1.4% agarose gel containing 6% (v/v) formaldehyde, and electrophoresis was performed as described³¹. RNA was visualized with ethidium bromide. The amount of 18S rRNA in each fraction of the gradient was quantified with ImageQuant 5.2 software (Molecular Dynamics).

Northern blot analysis. For ribosome association of individual mRNAs, gel electrophoresis was performed after polyosome analysis and fractionation as described above. RNA was subsequently transferred to nitrocellulose membranes (Amersham Hybond–N, GE Healthcare) and further processed as described³¹. DNA oligonucleotides (Supplementary Table 2; X85, X96, X105, X114) were radio-labelled with PNK according to standard procedures. Probes were incubated with the membranes in hybridization buffer (6× saline sodium citrate (SSC), 0.1% SDS, 10× Denhardt's reagent) overnight at 42 °C. Membranes were subsequently washed three times with wash buffer (6× SSC, 0.1% SDS). Probe signals were visualized using a Molecular Dynamics Phosphorimager (GE Healthcare) and quantified with ImageQuant 5.2 software (Molecular Dynamics). Normalized signal intensities were compiled for fractions corresponding to monosomes, light and heavy polysomes and averaged from at least three biological replicates.

Western blot analysis. Lysates from yeast strain A14201 at vegetative phase and stage 11 (ndt80 release time course) were prepared as described¹⁵. After loading equal amounts of protein on a 10% NEXT gel, denaturing gel electrophoresis and transfer to a PVDF membrane, western blotting was performed with anti-Ded1p (rabbit; 1:5,000) and anti-hexokinase (rabbit; 1:10,000; US Biological) antibodies.

Chemiluminescence was quantified by Imagequant software. Hexokinase served as a loading control for normalization.

Ribosome profiling. Yeast cultures (500 ml) were grown at 30 °C in rich medium to mid-log phase (OD_{600 nm} of approximately 0.4) and divided into two equal volumes. Cycloheximide (final concentration, 50 µg ml⁻¹) was added to one sample. Cells were rapidly collected by centrifugation at 4,000g for 2 min, and snap-frozen on dry ice. One volume of pre-warmed medium (44 °C) was added to the remaining sample, resulting in a temperature of 37 °C for the entire volume. The temperature of 37 °C was verified. The entire sample was immediately moved to a shaking incubator at 37 °C. Five minutes after temperature shift, the yeast culture was treated with cycloheximide and cells were collected as mentioned above. For run-off experiments, yeast cells were collected in the absence of cycloheximide (Extended Data Fig. 3e).

Cell lysis, RNase I treatment (Ambion) and sucrose gradient centrifugation was performed as described³² for 25 units A₂₆₀ per sample. In addition, lysates (approximately 150 µl) were treated with 3.25 µl Turbo DNase I for 1 h at 25 °C. Purification and processing of ribosome-protected fragments were carried out as described³², except that rRNA depletion with the RiboZero kit (Illumina) was omitted. Depletion of rRNA was performed at the level of circularized cDNA, as described⁷ (1 µl of a 5 µM mix of biotinylated DNA oligonucleotides, Supplementary Table 2 (X66–X80) and MyOne Streptavidin C1 DynaBeads (Invitrogen)). PCR amplification and sequencing was performed as described⁷.

Monosome-protected fragments were isolated as described¹². In brief, sucrose gradient centrifugation of lysates was performed and fractions corresponding to monosomes were pooled and treated with 1/10 U RNase I per unit A_{260 nm} lysate and 0.4U Turbo DNase I per unit A_{260 nm} lysate for 1 h at 25 °C. Reactions were stopped by phenol–chloroform extraction of RNA. Monosome-protected fragments were processed as described above for ribosome-protected fragments.

The fragmented mRNA control libraries were generated as described³². Sizing, concentration and quality of each DNA library was assessed with the High Sensitivity DNA kit on an Agilent2100 Bioanalyzer system. Up to eight DNA libraries were pooled before performing 50 bp single end read sequencing on an Illumina HiSeq2500 V2 in rapid run mode.

Processing of the ribosome profiling data was performed as described³². In brief, adaptor sequences and ribosomal reads were removed. Remaining reads were mapped to the sacCer3 genome with the TopHat software (parameters set as: --no-novel-juncs -N 2 --read-edit-dist 2 --max-insert-length 3 --max-deletion-length 3 -g 2 (<https://www.yeastgenome.org/>)). All other parameters were kept at default settings³³. The abundance of mRNAs in ribosome or monosome-protected fragments as well as in the fragmented RNA control libraries were determined using Cufflinks software³³. These values were used to calculate translational efficiencies as described¹⁴. For the calculation of log₂ΔTE values we also included a constant factor reflecting the change in the overall size of the mRNA pool, derived from the spike-in of RNA controls (Supplementary Table 3).

P-sites in ribosome-protected fragments (RPFs) were determined using the 13th position from the 5' end of reads with 28 or 29 nt¹⁴. The fraction of ribosomes on 5' UTRs was calculated for each mRNA by counting all RPFs on the 5' UTR (excluding positions –3 to –1), divided by the number of all RPFs mapped to the entire mRNA. mRNAs with 5' UTRs containing fewer than 10 nt were excluded from the analysis. The centre of ribosome density (CRD) was calculated as described³⁴. The shift in the CRD (ΔCRD) in *ded1*-95 compared to wild-type *DED1* upon temperature shift was defined relative to the entire length of the mRNA according to:

$$\Delta \text{CRD} = ((\text{CRD } \text{ded1}-95) - (\text{CRD wild-type } \text{DED1})) / \text{mRNA length}$$

A negative ΔCRD value marks increased ribosome accumulation in the 5' UTR in *ded1*-95.

ATIS were identified according to a previously described algorithm¹⁵. In brief, a position is considered an ATIS, (i) if minimal ribosome count value (± 1 nt of the nucleotide under consideration) is greater than nine (high-stringency ATIS) or four (medium-stringency ATIS) in all replicates; (ii) if the ratio of ribosome occupancy between two neighbouring nucleotides 5' to 3' (positionⁿ⁻¹/positionⁿ) is greater than or equal to three (high-stringency ATIS) in all replicates, or greater or equal of three in one and greater than or equal to 1.75 in the other replicate (medium-stringency ATIS); and (iii) if the normalized ribosome count in *ded1*-95 cells 5' after temperature shift to 37 °C is 1.5-fold higher than in wild-type *DED1* in all replicates. This algorithm identified 396 high-stringency ATIS and 2,126 medium-stringency ATIS. Near-cognate codons were identified in 259 high-stringency ATIS (65%) and 1,382 medium-stringency ATIS (65%) within a moving window of ± 1 nt. Canonical AUG initiation codons were found in 4% high-stringency ATIS, and in 3% medium-stringency ATIS. As a control set, we collected all near-cognate codons on 5' UTRs of mRNA genes with a 5' UTR length between 20 and 500 nt. After removal of near-cognate codons in medium-stringency ATIS, we identified 6,666 near-cognate codons.

XL-RAP-seq. Yeast cells containing HTBH-tagged *DED1* were grown in rich medium to an OD_{600 nm} of 1.0–1.5, collected by brief centrifugation at 4,000g, re-suspended in ice-cold water or remaining YPD medium, transferred to a Petri dish, and subjected to UV-light in a Stratalinker (600 mJ cm⁻², 254 nm) on ice. Cells were washed in ice-cold water, sedimented by centrifugation for 5 min at 5,250g, frozen on dry ice and stored at –80 °C.

Frozen cells were lysed in QIA-1M buffer (100 mM NaH₂PO₄ pH 8, 10 mM Tris, 1 M NaCl, 8 M Urea, 10 mM imidazole, 0.5% (w/v) IGEPAL, 2.5 mM β-mercaptoethanol, 1 mM PMSF, protease inhibitor cocktail (Roche)) with glass beads six times for 30 s in a Beadbeater system (Biospec products). Glass beads were removed, and lysates were centrifuged at 5,250g for 30 min. Cleared lysates were incubated with Ni²⁺-Agarose (40 µl slurry per g dry pellet weight, pre-equilibrated in buffer QIA-1M; Qiagen) overnight at 4 °C. Ni²⁺-beads were washed in 25 ml of wash buffer 1 (0.3 M NaCl, 10 mM Tris, 100 mM NaH₂PO₄, 8 M Urea, 10 mM imidazole) and sample was eluted with 10 ml elution buffer 1 (0.3 M NaCl, 100 mM Tris, 50 mM NaH₂PO₄, 8 M Urea, 500 mM imidazole, 10% (v/v) glycerol). Eluates were then incubated with 12.5 µl equilibrated streptavidin-conjugated agarose resin (Pierce Technologies) per g dry pellet weight overnight at 4 °C. Streptavidin beads were washed with 12.5 ml wash buffer 2 (0.3 M NaCl, 100 mM Tris, 8 M Urea, 0.5 mM EDTA)—containing 2% SDS, with wash buffer 2 (12.5 ml) without SDS, and with 1× TEV buffer. Beads were next incubated with 50 U AcTEV (Invitrogen) for 2 h at 4 °C. The sample was eluted with 2 × 0.9 ml TEV elution buffer (300 mM NaOAc pH 6, 8 M Urea, 0.5% NP-40). Eluates were incubated with 175 µl Proteinase K (4 mg ml⁻¹; Roche), and the reaction was stopped by standard phenol-chloroform extraction. Released RNA was precipitated by ethanol precipitation overnight. RNA was re-suspended in 1× Turbo DNase buffer and incubated with 0.4 µl TurboDNase (Ambion) in a final volume of 20 µl for 20 min at 37 °C. Turbo DNase was inactivated according to the manufacturer's instruction and the RNA was precipitated with ethanol.

cDNA was generated from the RNA sample using the 'template switch' activity of M-MLV reverse transcriptase³⁵. Reactions were performed in 20 µl according to the instructions of the manufacturer mix (Invitrogen) with 0.5 µl Superscript II and 0.05 µM final concentration of tailed random hexamer primer (X13, Supplementary Table 2). Reaction conditions were as follows: 20 °C, 10 min; 37 °C, 10 min; 42 °C, 45 min. Next, 0.25 µM of primers (X14–X17, Supplementary Table 2) containing a 7-nt index and three guanosine ribonucleotides at their 3' end were added to the reaction mix and reactions were performed at 42 °C for 30 min. Four microlitres of the resultant cDNA were used as template for amplification with primers X18 and X19 (Supplementary Table 2) and Advantage 2 polymerase mix (Clontech) for 30 cycles, according to the manufacturer's instructions. PCR products were precipitated and washed with 75% ethanol. DNA libraries were sequenced as 36-bp single-end reads on an Illumina Genome Analyzer. Reads were mapped to SacCer2 genome with Bowtie software with default settings.

Reads were excluded from further analysis if their location was outside of the boundaries of an mRNA or other transcribed regions of the genome as previously defined³⁶. Genes were only considered to be bound by Ded1p, if more than 10 FPKM mapped to the respective mRNA gene.

iCLIP. iCLIP experiments were performed independently with two different approaches, (i) using Ded1p-HTBH and (ii) Ded1p-His₆-FLAG₃, both on the endogenous *DED1* allele. For iCLIP with Ded1p-HTBH, cell growth, cross-linking and tandem affinity purification on Ni²⁺-agarose and streptavidin beads was performed as described above for the XL-RAP-seq procedure. Streptavidin beads were washed twice in 1× PNK buffer and split into two samples (80%, L; 20%, H). 200 ng RNase I was added per gram dry pellet weight to the L-sample and 0.1 ng RNase I to the H-sample. The samples were incubated for 5 min at 37 °C on a rotator. Resins were subsequently washed with ~1.5 ml wash buffer 2 (2% (w/v) SDS), and then with 1.5 ml wash buffer 2 without SDS, and finally with 1.5 ml 1× PNK buffer. The supernatant was removed and beads were re-suspended in 67 µl RNase-free water, 3 µl alkaline phosphatase (NEB) and 2 µl RNasin (Roche), and incubated for 20 min at 37 °C. Beads were washed twice with 1.5 ml 1× PNK buffer.

3' ligation was performed by re-suspending the resin in 32 µl RNase-free water with 8 µl of 20 µM RL3 RNA Linker (Supplementary Table 3). Reactions were performed overnight at 4 °C in 40 µl, containing 22 µl RNase-free water, 8 µl 10× T4 RNA ligase buffer, 8 µl BSA (0.2 µg µl⁻¹), 3 µl T4 RNA ligase (all NEB).

The resin was washed with 1.5 ml 1× TEV-salt buffer (50 mM Tris pH 7.5, 300 mM NaCl, 0.5 mM EDTA, 1 mM DTT) and twice with 1.5 ml 1× PNK buffer. Beads were re-suspended in 64 µl RNase-free water, 8 µl 10× PNK Buffer, 4 µl ³²P-γ-ATP, 4 µl T4 PNK (all NEB). Reactions were performed for 50 min in a shaking thermoblock at 37 °C. Beads were washed twice with 1.5 ml TEV salt buffer and twice with 1.5 ml TEV-elution buffer. Beads were subsequently mixed with SDS loading dye and subjected to PAGE on a 10% NEXT gel (Amresco) according to the manufacturer's conditions. Gels were subsequently blotted with nitrocellulose membranes (Amersham Protran, GE Healthcare) and exposed to

X-ray film. RNA was then liberated by Proteinase K treatment as described³⁷. The purified RNAs were re-suspended in 89 µl RNase-free water, 11 µl 10× DNase I Buffer, 5 µl RNasin, 5 µl RQ1 DNase (all Promega) and incubated for 20 min at 37 °C. The reaction was stopped by standard phenol-chloroform extraction and RNA was ethanol-precipitated overnight.

The DNase-treated RNA was re-suspended in 1.4 µl RNase-free water, 0.2 µl 10 mM dNTPs, 1 µl 20 nM reverse transcription primer X97 (Supplementary Table 2), and incubated for 5 min at 65 °C. Next, 0.8 µl 5× first-strand buffer, 0.2 µl 1M DTT, 0.2 µl RNase Inhibitor, 0.2 µl Superscript III (all Invitrogen) were added and incubated for 30 min at 50 °C. RNA was degraded by alkaline hydrolysis (after addition of 0.5 µl of 1N NaOH and incubation at 98 °C for 15 min). After addition of loading buffer, cDNA was applied to 10% denaturing PAGE and staining with SYBR Gold. Fragments of 100–125 nt were cut from the gel. The gel slices were crushed and cDNA was recovered by incubation in 500 µl diffusion buffer (20 mM Tris-HCl pH 7.5, 250 mM NaOAc, 1 mM EDTA, 0.25% (w/v) SDS) overnight at 4 °C with subsequent ethanol precipitation.

The cDNA was suspended in 15 µl RNase-free water and circularized with CircLigase I (Epicentre) according to the manufacturer's instructions. The circularized cDNA was used for amplification with Phusion polymerase (NEB) and primers X98 and X99 (Supplementary Information 2). PCR settings were: 30 s at 98 °C and then 24 PCR cycles (10 s at 98 °C, 30 s at 58 °C, 30 s at 72 °C). PCR products were applied to 10% non-denaturing PAGE and visualized by SYBR Gold. Products with 75–90 bp were extracted from cut gel slices, and ethanol precipitated as described above. PCR products were amplified with Phusion polymerase and primers X100 and X101 for five cycles using the same PCR settings as above. PCR products were then separated on a 2% agarose gel, cut out and subjected to Illumina sequencing using primer X102.

For iCLIP with Ded1p-His₆-FLAG₃, cells were grown in SD-Trp medium to OD_{600 nm} = 0.5–0.6. The culture was subsequently transferred to a 245 mm × 245 mm × 25 mm square Petri dish. UV cross-linking was performed in a Stratalinker 2400 (600 mJ cm⁻², 254 nm) at room temperature. Cells were collected by centrifugation for 5 min at 2000g, washed twice in ice-cold PBS, frozen in liquid nitrogen, and stored at –80 °C.

Frozen cells were lysed in CLIP lysis buffer (50 mM Tris-HCl, pH 7.8, 300 mM NaCl, 1% Triton X-100, 1 mM PMSF, protease inhibitor cocktail (Roche)) with glass beads six times for 1 min in a Disruptor Genie system (Scientific Industries). Lysates were centrifuged after removal of the glass beads at 10,000g, twice for 5 min. Cleared lysates (~26.5 A₂₆₀ units) were incubated with anti-FLAG M2 Magnetic Beads (20 µl slurry pre-equilibrated in CLIP Lysis Buffer; Sigma) in a total volume of 1 ml overnight at 4 °C. Beads were washed twice in 1 ml FLAG Wash Buffer (50 mM Tris-HCl pH 7.8, 1 M NaCl, 0.1% NP-40) and twice in 1 ml FLAG Elution Buffer (50 mM Tris-HCl pH 7.8, 150 mM NaCl, 0.1% NP-40). Proteins were eluted twice in 95 µl FLAG Elution Buffer containing 150 ng µl⁻¹ 3× FLAG tag peptide (Sigma). Pooled eluates were incubated with 10 µl RNase I (Ambion), diluted 1:500,000 in FLAG elution buffer for 15 min at room temperature. Reactions were quenched with 960 µl 8 M guanidine-HCl, 90 µl Dilution Buffer (600 mM Tris-HCl pH 7.8, 3.93 M NaCl), 6.4 µl 2 M imidazole, 10.8 µl 10% NP-40 and 12.8 µl 500 mM β-mercaptoethanol. RNase-treated eluates were incubated further with Ni-NTA magnetic agarose beads (50 µl slurry pre-equilibrated in Ni-NTA binding buffer (50 mM Tris-HCl pH 7.8, 300 mM NaCl, 10 mM imidazole, 6 M guanidine-HCl, 0.1% NP-40, 5 mM β-mercaptoethanol); Qiagen) overnight at 4 °C.

Ni²⁺-beads were washed twice in 1 ml CLIP wash buffer I (50 mM Tris-HCl pH 7.8, 500 mM NaCl, 10 mM imidazole, 6 M guanidine-HCl, 0.1% NP-40, 5 mM β-mercaptoethanol) and three times in 1 ml 1× PNK Buffer (50 mM Tris-HCl pH 7.8, 10 mM MgCl₂, 0.5% NP-40, 10 mM β-mercaptoethanol). Beads were subsequently incubated with 30 µl dephosphorylation mix (50 mM Tris-HCl pH 7.8, 10 mM MgCl₂, 10 mM β-mercaptoethanol, 3 M BU TSAP (Promega), 30 U SUPERase-In (Ambion)) for 30 min at 37 °C in a thermomixer at 1000 rpm. Reactions were terminated by adding 1 ml CLIP wash buffer I, and beads were washed three times in 1 ml 1× PNK buffer, re-suspended in 30 µl ligation mix (50 mM Tris-HCl pH 7.8, 10 mM MgCl₂, 10 mM β-mercaptoethanol, 10% PEG8000 (NEB), 10% DMSO, 2 µM 3' adenylated adaptor X103, 30 U T4 RNA Ligase 1 (NEB), 30 U SUPERase-In (Ambion)) and incubated for 3 h at 22 °C in a thermomixer at 1000 rpm. Reactions were terminated by adding 1 ml CLIP wash buffer I. Beads were washed three times in 1 ml 1× PNK Buffer, re-suspended in 30 µl Kinase Mix (50 mM Tris-HCl, pH 7.8, 10 mM MgCl₂, 10 mM β-mercaptoethanol, 30 U PNK (NEB), 5 µCi γ-³²P-ATP, 30 U SUPERase-In (Ambion)) and incubated for 30 min at 37 °C in a thermomixer (1000 rpm). Reactions were terminated by adding 1 ml CLIP Wash Buffer I. Beads were washed three times in 1 ml CLIP Wash Buffer I, and three times in 1 ml CLIP wash buffer II (50 mM Tris-HCl, pH 7.8, 50 mM NaCl, 10 mM imidazole, 0.1% NP-40, 5 mM β-mercaptoethanol).

Proteins were eluted with 35 µl CLIP wash buffer II containing 200 mM imidazole three times for 5 min at 22 °C in a thermomixer (1000 rpm).

Pooled eluates were digested with Proteinase K (Invitrogen) at 50 °C for 1 h. The reaction was stopped by standard phenol–chloroform extraction. Released RNA was precipitated by ethanol precipitation overnight in the presence of 1 µl GlycoBlue (Ambion) and 1 pmol reverse-transcription DNA primer X104. RNA was converted to first-strand cDNA in a 10 µl standard reaction mix with 0.5 µl Superscript III (Invitrogen) and the co-precipitated DNA primer. The reaction conditions were as follows: 25 °C for 5 min, 42 °C for 20 min, 50 °C for 40 min. RNA was degraded with 1.67 µl of 1 M NaOH for 10 min at 90 °C. The cDNA was ethanol precipitated with GlycoBlue for >2 h. cDNA fragments of 120–200 nt were gel purified on a urea-denaturing 6% acrylamide gel and ethanol precipitated with GlycoBlue overnight. cDNA was circularized in a 10 µl reaction mix using 0.5 µl CircLigase I (Epicentre) in the presence of 1 M betaine at 60 °C for 1 h. The reaction was then supplemented with additional 0.5 µl CircLigase I and incubated at 60 °C for 1 h. The enzyme was inactivated at 80 °C for 10 min. PCR and formamide-gel purification of PCR products were performed as described³⁸, using 20 cycles of PCR and isolating 120–200 nt ssDNA fragments.

Sequencing reads were processed as previously described^{37,39}. In brief, after the trimming of adaptor sequences, reads were mapped to sacCer3 with Bowtie2 or TopHat software with similar settings used for the ribosome profiling data, outlined above. Identical reads were subsequently collapsed and duplications removed. The cross-link position of Ded1p to RNA was defined as 1 nt 5' of the 5' mapped nucleotide of a sequencing read³⁷.

DMS-MaPseq. Yeast strains (wild-type DED1 and *ded1-95*) were grown in YPD at 30 °C. Overnight cultures were diluted to OD_{600 nm} of ~0.09 and grown to an OD_{600 nm} = 0.6. An equal volume of 44 °C YPD medium was added to achieve an immediate temperature shift to 37 °C, as outlined for the ribosome profiling experiments. Cultures were incubated in a 37 °C water bath for 3 min. At this time, DMS (Sigma) was added to a 5% (v/v) final concentration and incubation was continued with stirring for 3 min. DMS was quenched by adding 30 ml of ice-cold stop solution (30% β-mercaptoethanol, 50% (v/v) isoamyl alcohol). Cells were quickly transferred to ice, collected by centrifugation at 3,500g at 4 °C for 4 min, and washed with 10 ml 30% β-mercaptoethanol solution. Cells were re-suspended in 0.6 ml RNA lysis buffer (6 mM EDTA, 45 mM NaOAc, pH 5.5). Total RNA was purified with hot acid phenol (Ambion) and ethanol precipitation. Sequencing libraries were prepared as previously described¹⁷.

Raw fastq files were stripped of linker sequences and filtered for overall quality using the FASTX-Toolkit Clipper and Quality Filter functions (http://hannonlab.cshl.edu/fastx_toolkit/), respectively, requiring that 80% of sequenced bases have a quality score >25. Reads were aligned against the yeast genome (sacCer3) using Tophat v2.1.0 with Bowtie2 with the following settings for a 50 bp sequencing run: --no-novel-juncs -N 5 --read-gap-length 7 --read-edit-dist 7 --max-insertion-length 5 --max-deletion-length 5 -g 3. All non-uniquely aligned reads were then removed. Owing to empirically determined mutation enrichment from non-template addition, 2 nt was trimmed from the 5' end of each read. Mismatches located within 3 nt of an indel were also discarded for future analysis.

Bioinformatic analyses. Yeast genomic sequence conservation scores were obtained from *S. cerevisiae* genome database (<https://www.yeastgenome.org>). Positional coordinates of mRNAs including transcription start sites and polyadenylation sites are based on sacCer3 and reported measurement⁴⁰. Genome-wide datasets were visualized by IGV software⁴¹. Structural models of the small and large ribosomal subunits including initiation factors were generated with the Chimera software^{30,42}. Analyses of Gene Ontology term enrichment were carried out with GORilla software using a single ranked list of genes⁴³.

RNA structure prediction was carried out with sequences 0–99 nt 3' of the first nucleotide of an alternative start codon using the RNAfold web server⁴⁴. Constraint settings were derived from DMS-MaPseq data as follows: a nucleotide was set as ‘unpaired’ if the DMS-MaPseq counts of a given nucleotide exceeded the value of 0.49 relative to the third highest count number in the range of 100 nt downstream of an ATIS.

Statistical significance of enrichment or depletion in certain regions (for example, Figs. 2c, 3d, e, Extended Data Fig. 10a) was determined by comparing weighted data vectors of the observed variable to the background value. To this end, we calculated *t*-values with the *wtdd.t.test* function in R. The algorithm is based on the mean and 1/(standard errors)² as an estimate of the means accuracy. The given *P* values correspond to a two-tailed *t*-test.

Further bioinformatic analyses and multiple linear regressions were performed with R⁴⁵ with customized scripts using RStudio Software (<https://www.rstudio.com/>). Code is available upon request. Normalization of the datasets including ribosome protected fragments, monosome-protected fragments, Ded1p iCLIP-seq and DMS-MaPseq counts were performed relative to the total number of counts of the entire mRNA⁴².

To compute Ded1p binding density, DMS-MapSeq ratios, or sequence conservation values in the vicinity of ATIS, it was important to normalize for

inherent positional trends within the exact region in the respective iCLIP, DMS-MapSeq and sequence conservation datasets. For example, values for DMS-MapSeq ratios (counts *ded1-95*/counts wild type), and iCLIP reads show an upward trend with increasing distance from the 5' cap in 5' UTRs. To normalize for inherent positional trends, we calculated a background distribution for the vicinity of each ATIS. We randomly choose a position in the respective section of a given mRNA, and determined the signal distribution in the vicinity of this position (for example, position –5 relative to the 5' nt of an ATIS). This process was repeated four times. The background value reflects the average of these five calculated values. Reported enrichment values represent the ratio of the measured signal over the background value at each indicated position. Values are given in all plots as log₂(measured signal/background signal). Statistical significance of enrichment or depletion was determined by calculating the *t*-value of the observed variable on the basis of the mean and s.d. of the background value.

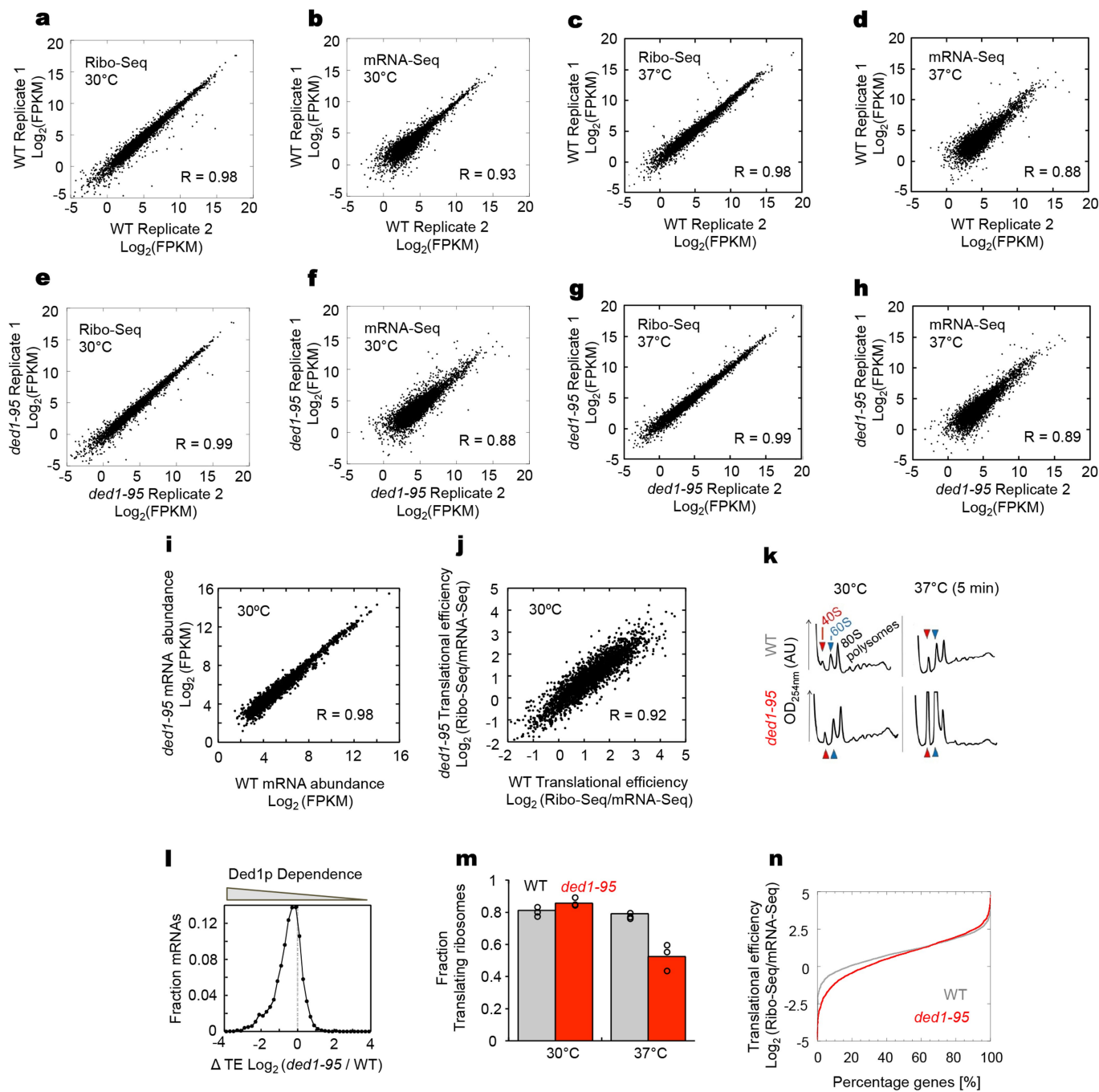
Metagenome profiles were calculated by averaging normalized Ded1p iCLIP counts and DMS-MaPseq counts after binning transcript coordinates from 5' UTRs, ORFs and 3' UTRs in bins reflecting 2% of each section of mRNA. Ded1p binding sites and the midpoint of RNA secondary structures were determined by Piranha peak calling software (<http://smithlabresearch.org>).

Calling parameters were optimized on the basis of visual inspection. To call peak sites of RNA secondary structures, a genome-wide dataset of log₂(counts of DMS-MaPseq wild type/*ded1-95*) was used as input file.

Reporting summary. Further information on experimental design is available in the Nature Research Reporting Summary linked to this paper.

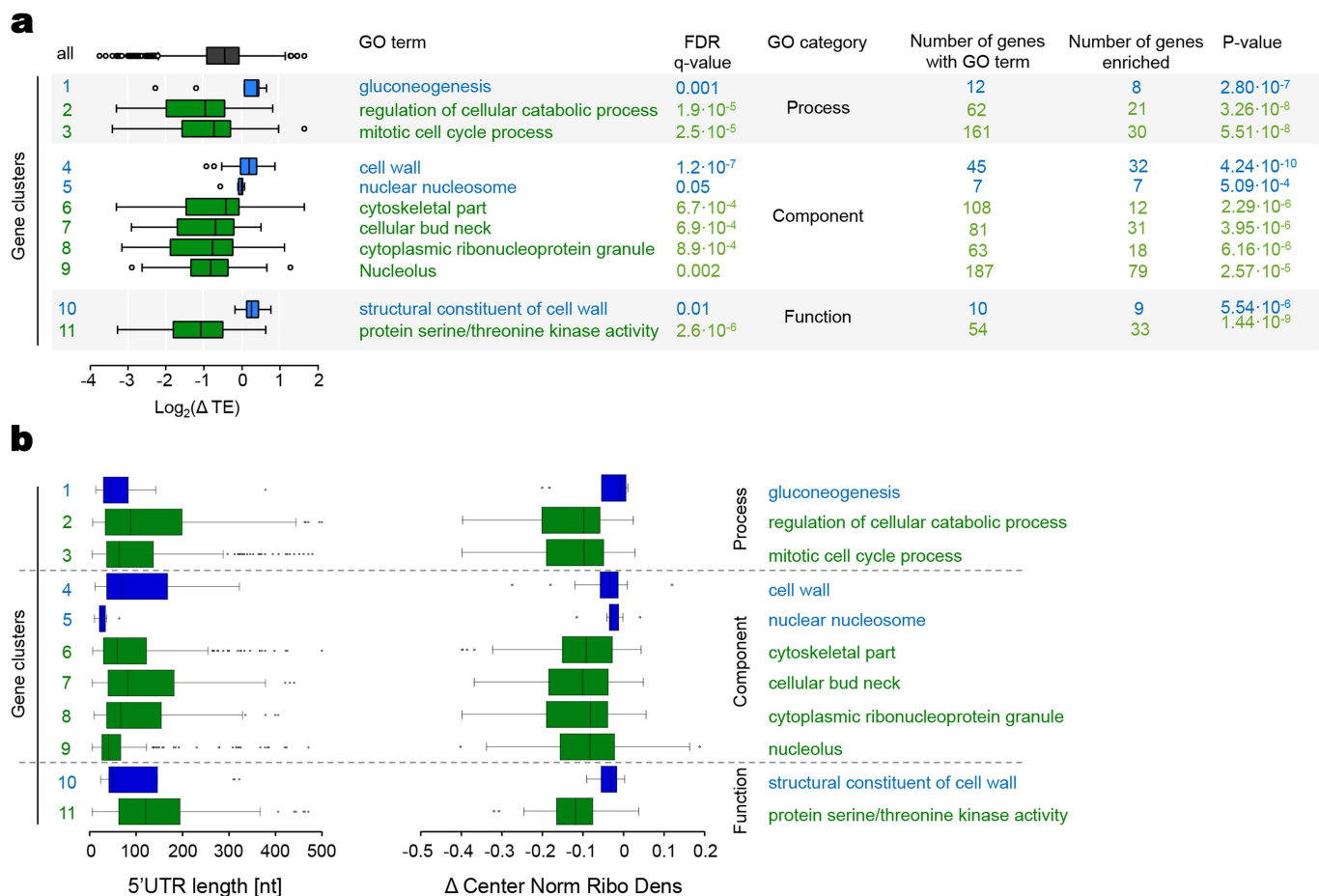
Data availability. The data that support the findings of this study have been deposited in the Gene Expression Omnibus (GEO) repository with the accession code GSE93959. All other data are available from the corresponding author upon reasonable request.

31. Hu, W., Sweet, T. J., Chamnongpol, S., Baker, K. E. & Coller, J. Co-translational mRNA decay in *Saccharomyces cerevisiae*. *Nature* **461**, 225–229 (2009).
32. Smith, J. E. et al. Translation of small open reading frames within unannotated RNA transcripts in *Saccharomyces cerevisiae*. *Cell Reports* **7**, 1858–1866 (2014).
33. Goecks, J., Nekrutenko, A. & Taylor, J. Galaxy: a comprehensive approach for supporting accessible, reproducible, and transparent computational research in the life sciences. *Genome Biol.* **11**, R86 (2010).
34. Andreev, D. E. et al. Translation of 5' leaders is pervasive in genes resistant to eIF2 repression. *eLife* **4**, e03971 (2015).
35. Matz, M. et al. Amplification of cDNA ends based on template-switching effect and step-out PCR. *Nucleic Acids Res.* **27**, 1558–1560 (1999).
36. Nagarashmi, U. et al. The transcriptional landscape of the yeast genome defined by RNA sequencing. *Science* **320**, 1344–1349 (2008).
37. König, J. et al. iCLIP reveals the function of hnRNP particles in splicing at individual nucleotide resolution. *Nat. Struct. Mol. Biol.* **17**, 909–915 (2010).
38. Subtelny, A. O., Eichhorn, S. W., Chen, G. R., Sive, H. & Bartel, D. P. Poly(A)-tail profiling reveals an embryonic switch in translational control. *Nature* **508**, 66–71 (2014).
39. Licatalosi, D. D. et al. HITS-CLIP yields genome-wide insights into brain alternative RNA processing. *Nature* **456**, 464–469 (2008).
40. Park, D., Morris, A. R., Battenhouse, A. & Iyer, V. R. Simultaneous mapping of transcript ends at single-nucleotide resolution and identification of widespread promoter-associated non-coding RNA governed by TATA elements. *Nucleic Acids Res.* **42**, 3736–3749 (2014).
41. Robinson, J. T. et al. Integrative genomics viewer. *Nat. Biotechnol.* **29**, 24–26 (2011).
42. Pettersen, E. F. et al. UCSF Chimera—a visualization system for exploratory research and analysis. *J. Comput. Chem.* **25**, 1605–1612 (2004).
43. Eden, E., Navon, R., Steinfeld, I., Lipson, D. & Yakhini, Z. GOrilla: a tool for discovery and visualization of enriched GO terms in ranked gene lists. *BMC Bioinformatics* **10**, 48 (2009).
44. Gruber, A. R., Bernhart, S. H. & Lorenz, R. The ViennaRNA web services. *Methods Mol. Biol.* **1269**, 307–326 (2015).
45. The R Core Team. *A language and environment for statistical computing*. R Foundation for Statistical Computing, Vienna, Austria, <http://www.R-project.org> (2013).
46. Benjamini, Y. & Hochberg, Y. Controlling the false discovery rate: a practical and powerful approach to multiple testing. *J. R. Stat. Soc. Series B Stat. Methodol.* **57**, 289–300 (1995).
47. Miyasaka, H. The positive relationship between codon usage bias and translation initiation AUG context in *Saccharomyces cerevisiae*. *Yeast* **15**, 633–637 (1999).
48. Nielsen, K. H. et al. Synergistic activation of eIF4A by eIF4B and eIF4G. *Nucleic Acids Res.* **39**, 2678–2689 (2011).
49. Floor, S. N., Condon, K. J., Sharma, D., Jankowsky, E. & Doudna, J. A. Autoinhibitory interdomain interactions and subfamily-specific extensions redefine the catalytic core of the human DEAD-box protein DDX3. *J. Biol. Chem.* **291**, 2412–2421 (2016).
50. Siepel, A. et al. Evolutionarily conserved elements in vertebrate, insect, worm, and yeast genomes. *Genome Res.* **15**, 1034–1050 (2005).



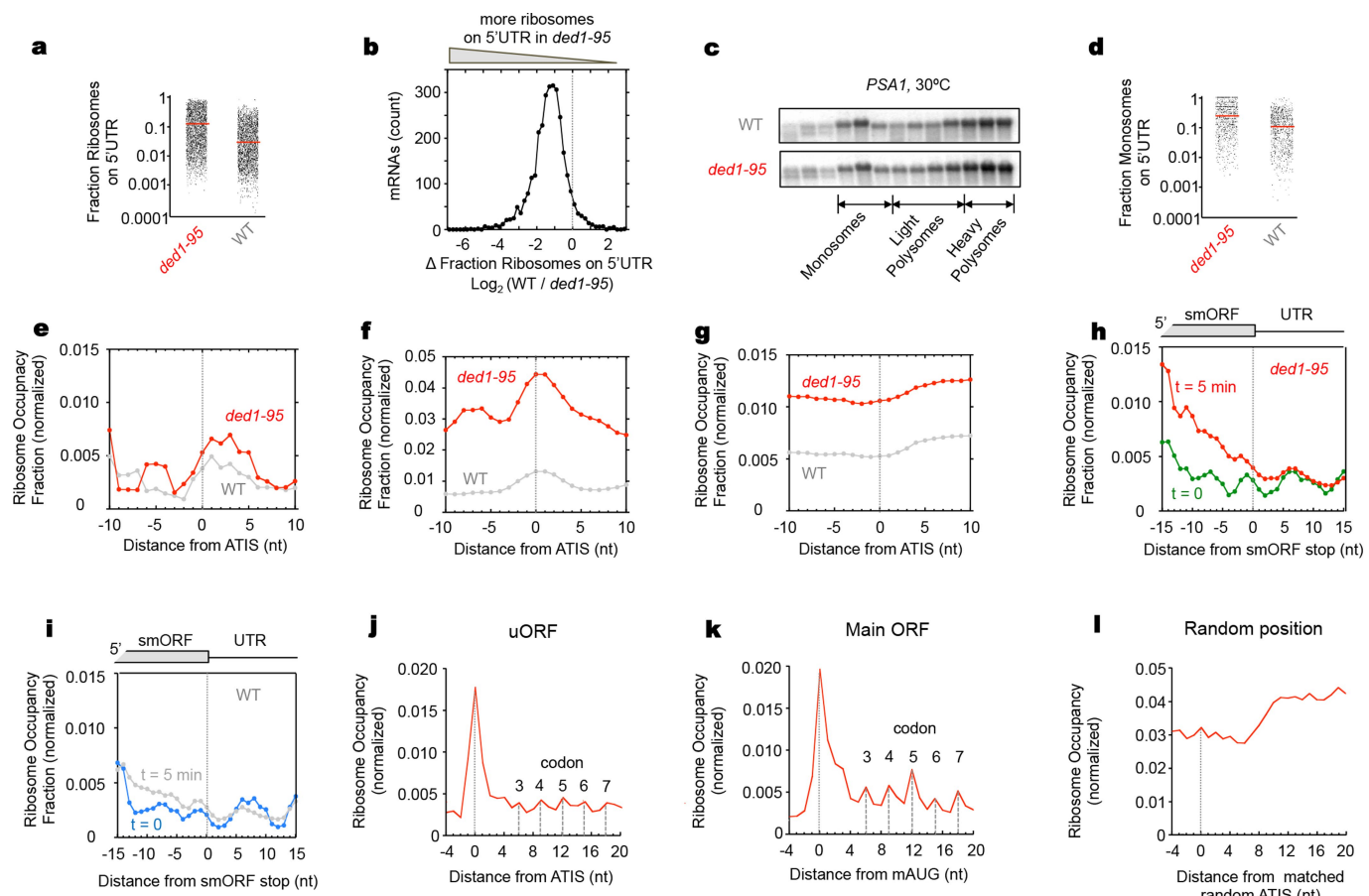
Extended Data Fig. 1 | mRNA expression, and translation profiles in wild-type *DED1* and *ded1-95*. **a**, Correlation of ribosome footprint counts between two biological replicates in wild-type *DED1* at 30 °C ($n = 5,523$). **b**, Correlation of mRNA expression levels between two biological replicates in wild-type *DED1* at 30 °C ($n = 5,372$). **c**, Correlation of ribosome footprint counts between two biological replicates in wild-type *DED1*, 5 min after temperature shift to 37 °C ($n = 5,523$). **d**, Correlation of mRNA expression levels between two biological replicates in wild-type *DED1*, 5 min after temperature shift to 37 °C ($n = 5,372$). **e**, Correlation of ribosome footprint counts between two biological replicates in *ded1-95* at 30 °C ($n = 5,523$). **f**, Correlation of mRNA expression levels between two biological replicates in *ded1-95* at 30 °C ($n = 5,372$). **g**, Correlation of ribosome footprint counts between two biological replicates in *ded1-95*, 5 min after temperature shift to 37 °C ($n = 5,523$). **h**, Correlation of mRNA expression levels between two biological replicates in *ded1-95*, 5 min after temperature shift to 37 °C ($n = 5,372$). **i**, Correlation

of mRNA expression levels between wild-type *DED1* and *ded1-95* at 30 °C ($n = 2,976$). Each data point represents the average of at least two replicates. **j**, Correlation of translational efficiencies between wild-type *DED1* and *ded1-95* at 30 °C ($n = 2,976$). Each data point represents the average of at least two replicates. **k**, Representative polysome profiles of wild-type *DED1* and *ded1-95* strains at 30 °C and 5 min after shift to 37 °C. Similar results were obtained in three independent experiments. **l**, Changes in translational efficiencies (Δ TE) for mRNAs in *ded1-95*, compared to wild-type *DED1*, 5 min after temperature shift (mean of two biological replicates). The dotted line indicates no change. **m**, Fraction of 18S rRNA in polysome fractions, compared to the entire sample, at 30 °C and 5 min after temperature shift to 37 °C. Each bar represents the average of three independent experiments. Empty circles represent each replicate. **n**, Cumulative distribution of translational efficiencies of wild-type *DED1* and *ded1-95*, 5 min after temperature shift to 37 °C ($n = 2,976$). Each data point represents the average of at least two replicates.



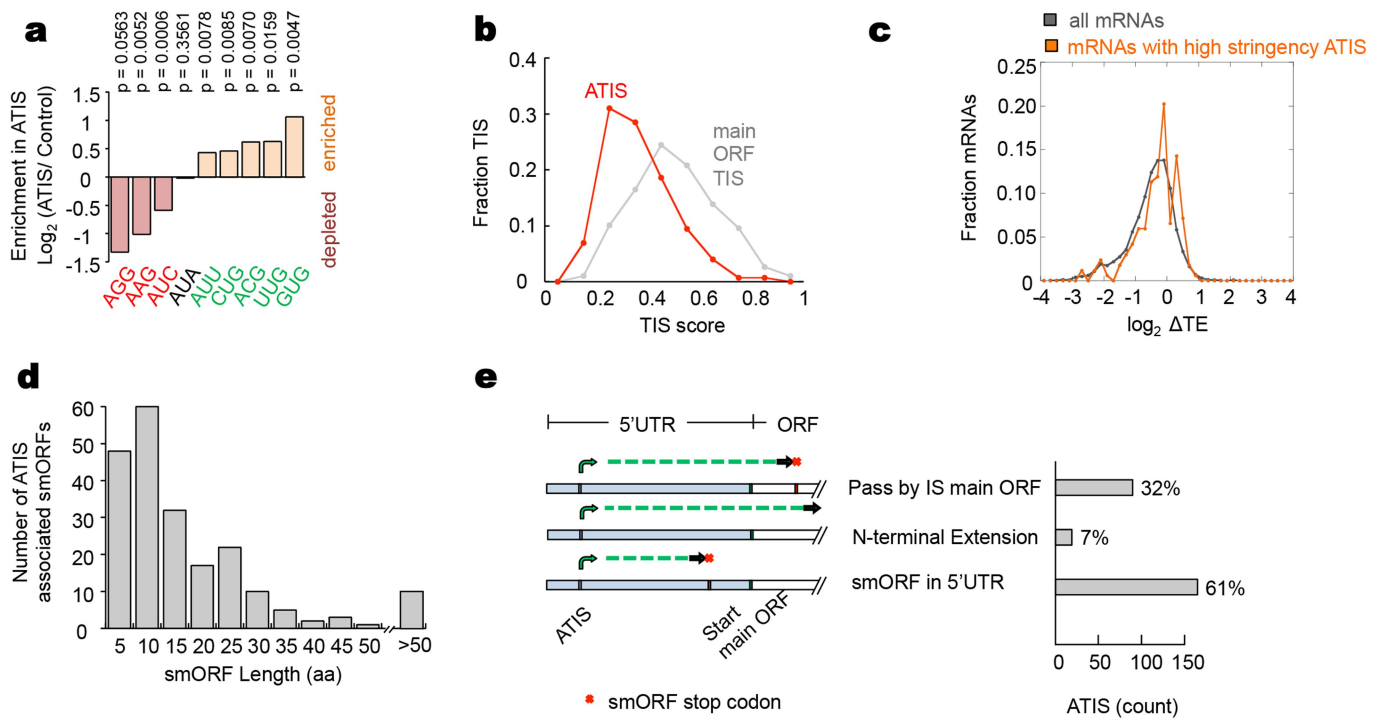
Extended Data Fig. 2 | A subset of mRNAs is largely insensitive to Ded1p. **a**, mRNA groups defined by Gene Ontology term with translation that is strongly affected (green) or largely unaffected by Ded1p (blue). Box plots (group median) of change in translational efficiencies. Box boundaries, upper and lower quartiles; error bars, $1.5 \times$ interquartile range. The black box plot marks changes in translational efficiencies for all mRNAs (Fig. 1b). mRNAs for each Gene Ontology term were extracted

from the *Saccharomyces* Genome Database (<https://www.yeastgenome.org>). The false discovery rate q value indicates the enrichment P value according to a hypergeometric model after correction for multiple testing using the Benjamini and Hochberg method⁴⁶. **b**, Box plots (as in a) of 5' UTR lengths and median of the shift in the normalized centre of ribosome density (Fig. 1b) for Gene Ontology term defined mRNA groups, colour-coded as in a.



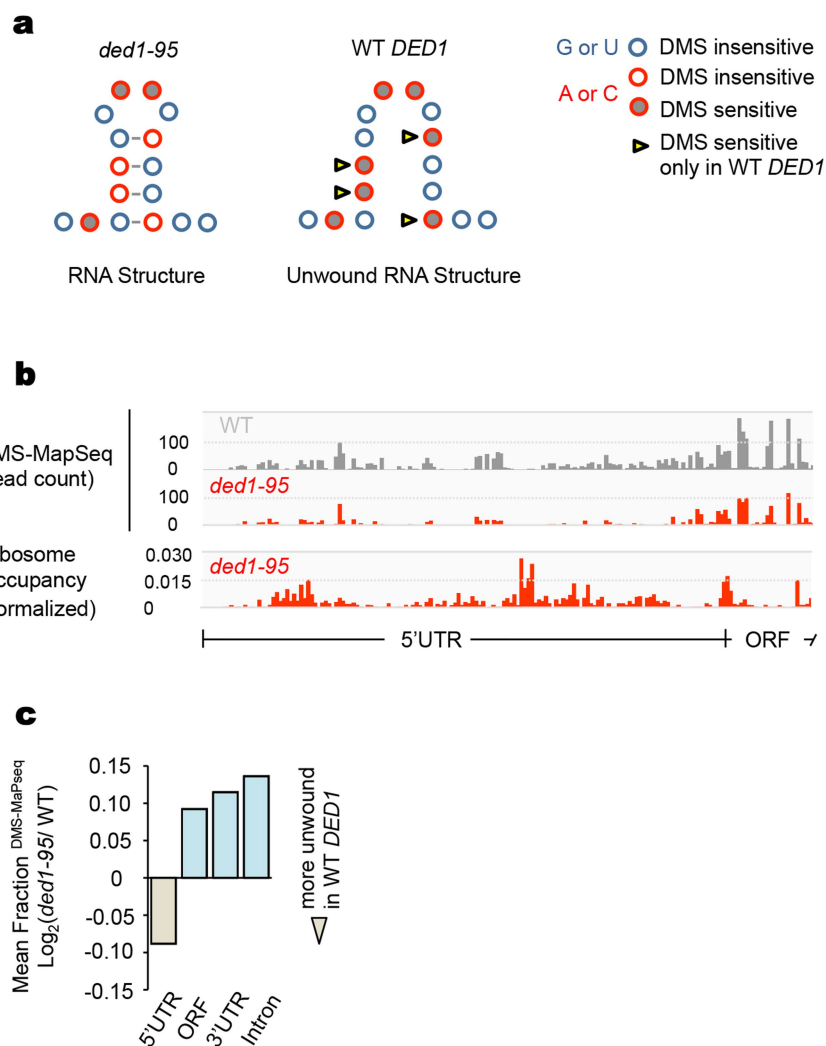
Extended Data Fig. 3 | Activation of ATIS in *ded1-95* upon temperature shift. **a**, Fraction of ribosome footprints on 5' UTRs in wild-type *DED1* and *ded1-95*, (5 min, 37 °C, $n = 3,273$). The red line indicates the mean. Statistical significance for the difference between *ded1-95* and wild-type *DED1*: $P = 1.2 \times 10^{-19}$ (two tailed *t*-test). A similar result was obtained in an independent replicate ($P = 5.4 \times 10^{-47}$). **b**, Changes in the fraction of ribosomes on 5' UTRs for all mRNAs ($n = 2,660$) in wild-type *DED1* compared to *ded1-95*, 5 min after temperature shift to 37 °C. The values on the *x*-axis represent the ratio (\log_2) of the fraction of ribosomes on each 5' UTR in the wild type, divided by the fraction of ribosomes on the same 5' UTR in *ded1-95*. Each value represents the mean of two independent biological replicates. **c**, Representative northern blots of PSA1 after sucrose gradient centrifugation for wild-type *DED1* and *ded1-95*, at 30 °C. A similar result was obtained in an independent biological replicate. **d**, Fraction of ribosome footprints on 5' UTRs in wild-type *DED1* and *ded1-95*, (5 min, 37 °C), measured only in 80S monosomes ($n = 973$, reads from two independent experiments combined). Statistical significance for the difference between *ded1-95* and wild-type *DED1*: $P = 1.2 \times 10^{-50}$ (two tailed *t*-test). **e**, Mean ribosome occupancy within 10 nt 3' and 5' of the high-confidence ATIS in 5' UTRs (moving average ± 1 nt, 5 min, 37 °C), measured without cycloheximide. **f**, Mean ribosome occupancy within 10 nt 3' and 5' of the high-confidence ATIS in 5' UTRs ($n = 274$) in 80S

monosomes (moving average ± 1 nt, 5 min, 37 °C). **g**, Mean ribosome occupancy within 10 nt 3' and 5' of all near-cognate initiation codons ($n = 61,614$; excluding medium-confidence ATIS) in 5' UTRs (moving average ± 1 nt, 5 min, 37 °C). **h**, Ribosome occupancy of 3' ends in small upstream open reading frames (smORFs) initiating at high-confidence ATIS in *ded1-95* before (*t* = 0) and after (*t* = 5 min) temperature shift. smORFs were included in this analysis if its length exceeds three codons and if the smORF terminates at least 11 nt upstream of the main AUG codon ($n = 76$). **i**, Ribosome occupancy of 3' ends of smORFs defined in **e** in wild-type *DED1* before (*t* = 0) and after (*t* = 5 min) temperature shift. **j**, Ribosome occupancy 4 nt 5' and 20 nt 3' of high-confidence ATIS on 5' UTRs ($n = 274$) for *ded1-95*, 5 min after temperature shift. The dashed lines indicate the first nucleotide of the marked in-frame codons. **k**, Ribosome occupancy 4 nt 5' and 20 nt 3' of the main AUG (mAUG) of mRNAs containing high-confidence ATIS on 5' UTRs for *ded1-95*, 5 min after temperature shift. For mRNAs with multiple high-confidence ATIS in their 5' UTR, the main AUG was counted only once. The dashed lines indicate the first nucleotide of the marked in-frame codons. **l**, Ribosome occupancy 4 nt 5' and 20 nt 3' of high-confidence ATIS-matched random positions (averaged from five randomizations) on 5' UTRs ($n = 274$) for *ded1-95*, 5 min after temperature shift. The dashed line indicates the first nucleotide.



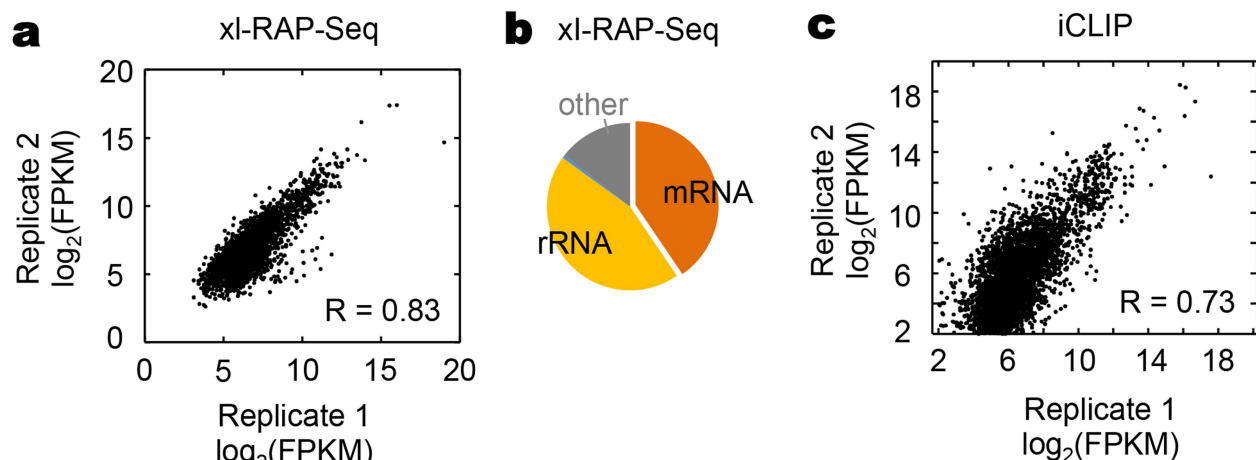
Extended Data Fig. 4 | Characteristics of small open reading frames associated with activated ATISs. **a**, Enrichment or depletion of each near-cognate codon in ATISs over the background distribution of the codon. *P* values determined using a two-tailed *t*-test. **b**, Mean translation initiation site score (positions -6 to $+6$, excluding $+1$ to $+3$), calculated according to previously published methods⁴⁷, for high-stringency ATIS ($n = 274$, red), and TIS of main ORFs ($n = 4,972$, grey). A TIS score exceeding 0.01 is considered a potential translational initiation site¹⁴. **c**, Changes in translational efficiencies (ΔTE) for mRNAs in *ded1-95*,

compared to wild-type DED1, 5 min after temperature shift for all mRNAs (Fig. 1b) and ATIS-containing mRNAs. **d**, Length of the small open reading frames (smORFs) associated with *ded1-95*-activated ATIS. smORFs encoding N-terminal extensions were excluded from the analysis. **e**, Type of smORFs associated with *ded1-95*-activated ATIS. The bar graphs show the fraction of smORFs that falls into each category. The distribution of changes in translation efficiency (ΔTE) for RNAs with each type of smORF did not differ significantly.



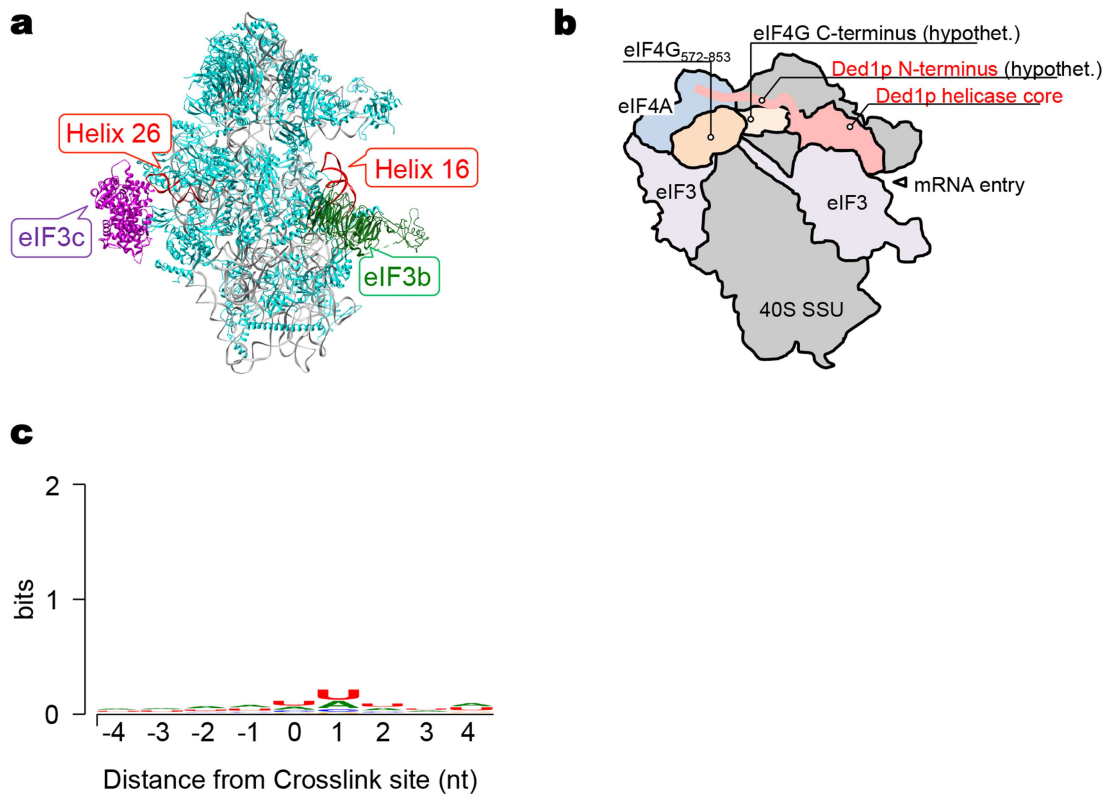
Extended Data Fig. 5 | mRNA structure unwinding by Ded1p in cells using DMS MaPSeq. **a**, Schematic for DMS-MaPseq approach to monitor RNA structure unwinding by Ded1p. All DMS-MaPseq experiments were performed 5 min after temperature shift. **b**, Representative DMS MaPSeq tracks in the *PSA1* 5' UTR 5 min after temperature shift for wild-type *DED1* (grey) and *ded1-95* (red). Bars show normalized reverse transcription stops. A similar result was obtained in an independent

replicate. The average Pearson's correlation coefficient of DMS-MaPseq counts per 5' UTR between two replicates (5 min after temperature shift to 37 °C) were $R = 0.57$ ($n = 864$) for the wild type and $R = 0.63$ ($n = 692$) for *ded1-95*. The ribosome occupancy track for *ded1-95* is shown for reference. **c**, Unwinding of mRNA structure by Ded1p for different mRNA regions. Similar results were obtained in two independent experiments.



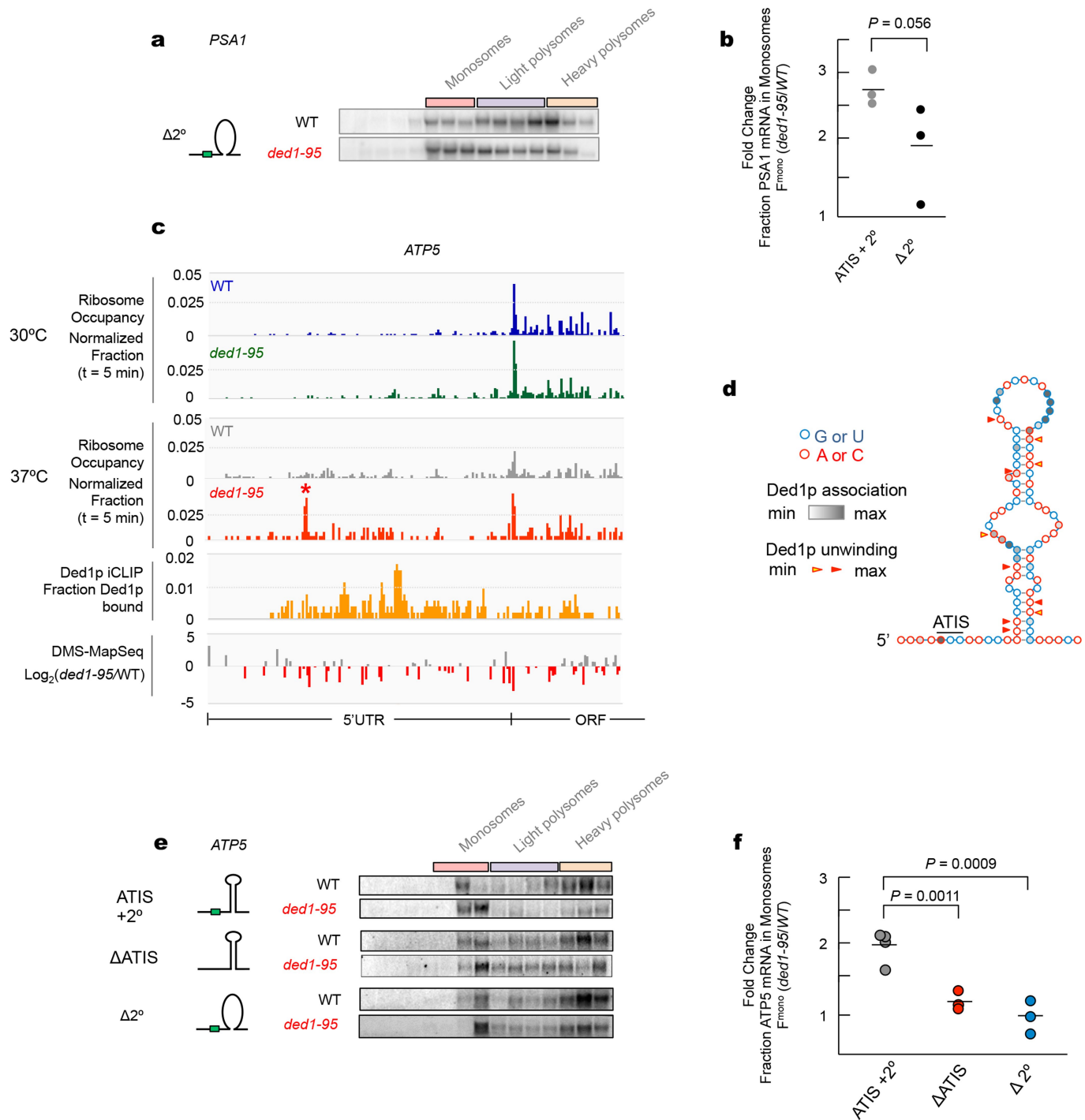
Extended Data Fig. 6 | XL-RAP-seq and iCLIP. **a**, Correlation of sequence reads (fragments per kilobase of exon per million fragments mapped, FPKM) per mRNA for two independent biological XL-RAP-seq replicates ($n = 2,992$). **b**, Fraction of mRNA (40%) and rRNA (44%) cross-linked to wild-type Ded1p as a fraction of all sequencing reads (mean of

two independent experiments). $n = 4,280$ mRNAs exceed a minimal read count of $\text{FPKM} \geq 10$. **c**, Correlation of the number of reverse transcription stops (FPKM) per mRNA for the two independent iCLIP approaches. Replicate 1, FLAG-tagged Ded1p; replicate 2, HTBH-tagged Ded1p; $n = 4,007$.



Extended Data Fig. 7 | Ded1p binding sites on 18S RNA and mRNAs.
a, Ded1p binding sites on helix 720 (exit) and helix 16 (entry) (red) are in close proximity to the binding sites of elf3c (purple) and elf3b (green) on the 40S ribosomal subunit⁴² (rRNA, grey; ribosomal proteins, cyan). **b**, Localization of Ded1p (apricot) on helix 16 of the PIC. Schematic model of the yeast PIC with elf3 (http://www.banggroup.ethz.ch/research/eukaryotic_translation_initiation.html and references therein); the positioning of elf4G⁵⁷²⁻⁸⁵³ and elf4A is derived from previously published work⁴⁸. The position of the elf4G C terminus is hypothetical. The helicase

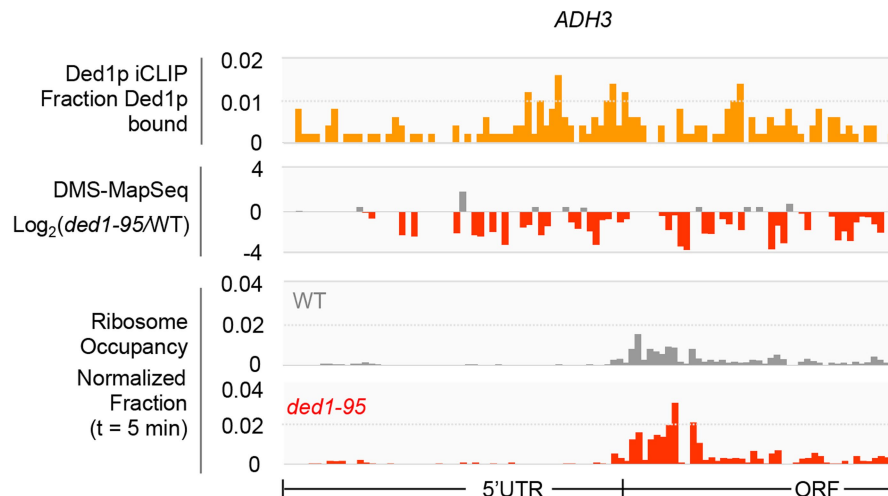
core of Ded1p was modelled in analogy to the DDX3 core structure⁴⁹, with the RNA binding site in contact with helix 16 at the main iCLIP cross-link sites. The position of the low-complexity N terminus of Ded1p is hypothetical. **c**, Sequence logo of Ded1p binding sites on mRNAs. Sets of 10^4 binding sites were randomly sampled from all Ded1p cross-linking sites and used as input to create a sequence logo (http://weblogo.berkeley.edu). All subsets yielded essentially the same sequence logo as shown here. Position zero denotes the reverse transcription stop.



Extended Data Fig. 8 | Representative northern blots of PSA1 ($\Delta 2^\circ$) and ATP5 (Δ ATIS, $\Delta 2^\circ$) for wild-type *DED1* and *ded1-95*.

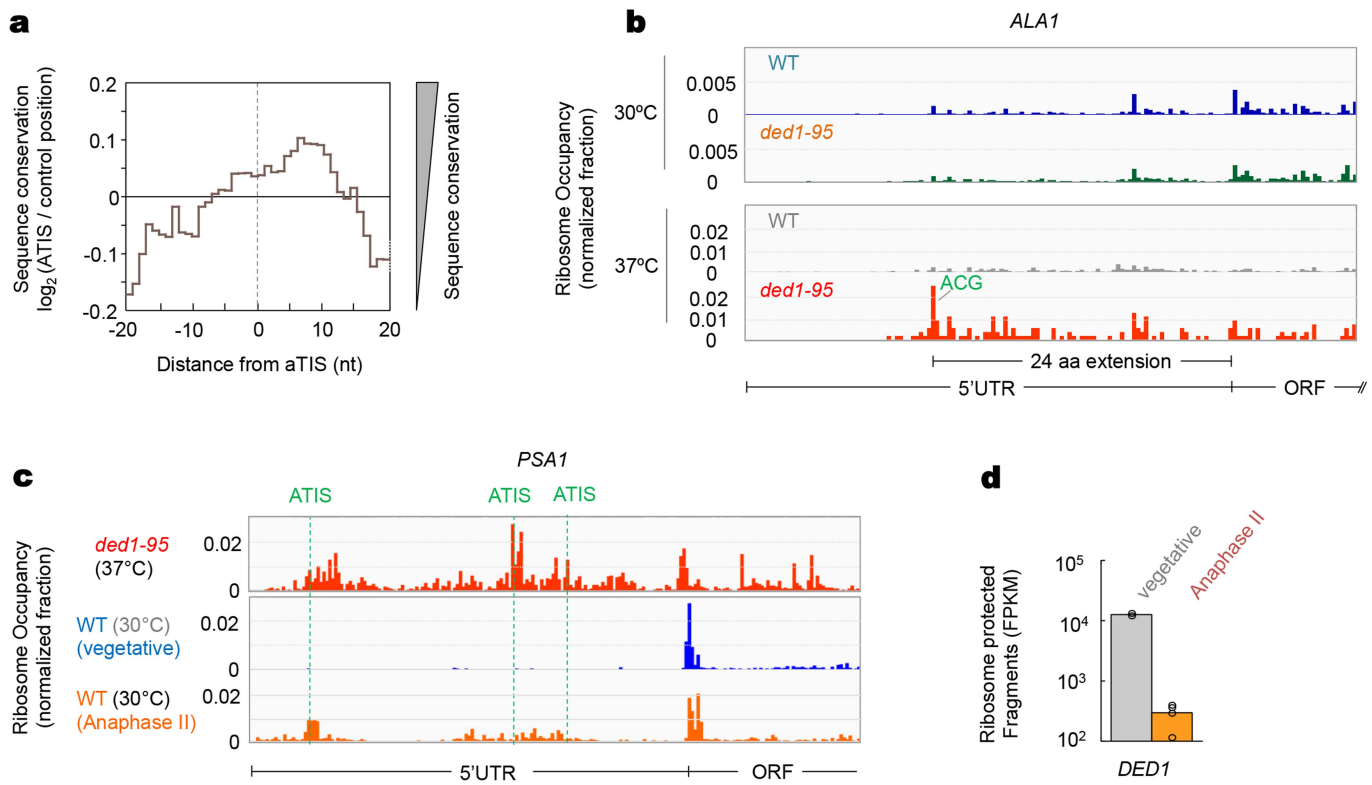
a, Representative RNA blots (5 min, 37 °C) for the *PSA1* mRNA with altered secondary structure, 3' of the ATIS ($\Delta 2^\circ$). Similar results were obtained in three independent biological replicates. **b**, Quantification of RNA blots for accumulation of the *PSA1* $\Delta 2^\circ$ mRNA in monosomes in *ded1-95*, compared to wild-type *DED1*. The line indicates the average. The *P* value for the difference in monosome accumulation was determined using a one-tailed *t*-test. **c**, Representative ribosome profiling tracks for the 5' UTR of *ATP5* in wild-type *DED1* and *ded1-95* (at 30 °C and after temperature shift). The near-cognate initiation codon is highlighted by a star. For comparison, Ded1p cross-linking (yellow track) and differential DMS-MapSeq tracks (log₂(*ded1-95*/wild type), unwound mRNA regions are marked by red bars and have negative values) for the 5' UTR of the *ATP5* mRNA are also shown. Similar results were obtained in two

independent experiments. **d**, DMS-MapSeq-constrained secondary-structure model of a fragment of the *ATP5* mRNA 5' UTR. The ATIS is marked by a line. Ded1p cross-linking (iCLIP) and unwinding (DMS-MapSeq) for each nucleotide are indicated. The ratio of normalized DMS-MapSeq counts of wild type/*ded1-95* in two categories: yellow triangles, 0.6 – 1.0 (moderately unwound) and red triangles, >1.0 (strongly unwound). **e**, Representative RNA blots (5 min, 37 °C) for wild-type *ATP5* mRNA and the same mRNA with mutations in the ATIS (Δ ATIS) or with altered secondary structure 3' of the ATIS ($\Delta 2^\circ$) for wild-type *DED1* and *ded1-95*. Similar results were obtained in three independent experiments. **f**, Quantification of RNA blots for accumulation of the *ATP5* Δ ATIS and $\Delta 2^\circ$ mRNA in monosomes in *ded1-95*, compared to wild-type *DED1*. Lines indicate averages and *P* values were determined using a one-tailed *t*-test.



Extended Data Fig. 9 | Ded1p binding and mRNA remodelling can occur without decreased translation efficiency if no near-cognate initiation codon is present. Ded1p iCLIP track, differential DMS-MaPseq track (5 min, 37 °C) and ribosome occupancy tracks (5 min, 37 °C) of wild-type *DED1* and *ded1-95* for *ADH3* mRNA, the translation of which is

largely unaffected by Ded1p ($\Delta TE = -0.1$). 5' UTR and ORF are marked. iCLIP and DMS-MaPseq tracks show Ded1p binding and remodelling of the 5' UTR, ribosome profiling tracks indicate no significant accumulation of ribosomes in the 5' UTR. Similar results were obtained in two independent experiments.



Extended Data Fig. 10 | ATIS conservation across fungi and Ded1p-mediated activation of upstream ORFs starting from near-cognate initiation codons. **a**, Sequence conservation in fungi around high-confidence ATIS (moving average of ± 1 nt). Positive values indicate higher sequence conservation than the average of five randomly chosen positions on the same 5' UTR for each ATIS, negative values indicate less sequence conservation (conservation scores were obtained from the sacCer3 phastCons7way dataset, on the basis of sequence homology between the following species: *S. cerevisiae*, *S. paradoxus*, *S. mikatae*, *S. kudriavzevii*, *S. bayanus*, *Naumovozyma castellii* and *Lachancea kluyveri*)⁵⁰. **b**, Ribosome occupancy tracks (30 °C and 5 min, 37 °C) of wild-type *DED1* and *ded1-95* for *ALA1* mRNA. 5' UTR and ORF are indicated. The ACG initiation codon (-25 , marked) has been previously shown to function as an ATIS for the mitochondrial isoform of *Ala1p*²⁹. Similar results were obtained in two independent biological replicates for each experiment. **c**, Ribosome occupancy tracks (5 min, 37 °C) of *ded1-95* and wild-type *DED1* (vegetative control and anaphase II) for *PSA1* mRNA. ATISs are marked by dashed lines. Similar results were obtained in two (vegetative control) and four (anaphase II) independent experiments. **d**, Ribosome-protected fragments mapping to *DED1* in vegetative cells and cells in anaphase II. Data are the mean of two (vegetative) and four (anaphase II) independent experiments, circles represent each replicate.

wild-type *DED1* and *ded1-95* for *ALA1* mRNA. 5' UTR and ORF are indicated. The ACG initiation codon (-25 , marked) has been previously shown to function as an ATIS for the mitochondrial isoform of *Ala1p*²⁹. Similar results were obtained in two independent biological replicates for each experiment. **c**, Ribosome occupancy tracks (5 min, 37 °C) of *ded1-95* and wild-type *DED1* (vegetative control and anaphase II) for *PSA1* mRNA. ATISs are marked by dashed lines. Similar results were obtained in two (vegetative control) and four (anaphase II) independent experiments. **d**, Ribosome-protected fragments mapping to *DED1* in vegetative cells and cells in anaphase II. Data are the mean of two (vegetative) and four (anaphase II) independent experiments, circles represent each replicate.

Reporting Summary

Nature Research wishes to improve the reproducibility of the work that we publish. This form provides structure for consistency and transparency in reporting. For further information on Nature Research policies, see [Authors & Referees](#) and the [Editorial Policy Checklist](#).

Statistical parameters

When statistical analyses are reported, confirm that the following items are present in the relevant location (e.g. figure legend, table legend, main text, or Methods section).

n/a Confirmed

- The exact sample size (n) for each experimental group/condition, given as a discrete number and unit of measurement
- An indication of whether measurements were taken from distinct samples or whether the same sample was measured repeatedly
- The statistical test(s) used AND whether they are one- or two-sided
Only common tests should be described solely by name; describe more complex techniques in the Methods section.
- A description of all covariates tested
- A description of any assumptions or corrections, such as tests of normality and adjustment for multiple comparisons
- A full description of the statistics including central tendency (e.g. means) or other basic estimates (e.g. regression coefficient) AND variation (e.g. standard deviation) or associated estimates of uncertainty (e.g. confidence intervals)
- For null hypothesis testing, the test statistic (e.g. F , t , r) with confidence intervals, effect sizes, degrees of freedom and P value noted
Give P values as exact values whenever suitable.
- For Bayesian analysis, information on the choice of priors and Markov chain Monte Carlo settings
- For hierarchical and complex designs, identification of the appropriate level for tests and full reporting of outcomes
- Estimates of effect sizes (e.g. Cohen's d , Pearson's r), indicating how they were calculated
- Clearly defined error bars
State explicitly what error bars represent (e.g. SD, SE, CI)

Our web collection on [statistics for biologists](#) may be useful.

Software and code

Policy information about [availability of computer code](#)

Data collection

Image Quant5.2 (Molecular Dynamics)

Data analysis

FASTX-Toolkit (NGS read processing), TopHat2.1.0 (read mapping for ribosome profiling), Cufflinks (NGS read counting for ribosome profiling), EXCEL (Data arrangement and manipulation), Custom Code (R, Python; aTIS identification and further data analysis), Bowtie2 (xLRAP, NGS read mapping), TopHat 2.1.0, Bowtie2 (NGS read mapping for iCLIP and DMS-MaPSeq), IGV genome browser (NGS data visualization), Chimera (Structure visualization), GOrilla (GO-term analysis), RNAfold web server (RNA secondary structure prediction), Piranha (NGS iCLIP and DMS-MapSeq, peak calling software), Weblogo (NGS iCLIP, sequence logo), Pymol (protein structure visualization). Kaleidagraph (Plots)

For manuscripts utilizing custom algorithms or software that are central to the research but not yet described in published literature, software must be made available to editors/reviewers upon request. We strongly encourage code deposition in a community repository (e.g. GitHub). See the Nature Research [guidelines for submitting code & software](#) for further information.

Data

Policy information about [availability of data](#)

All manuscripts must include a [data availability statement](#). This statement should provide the following information, where applicable:

- Accession codes, unique identifiers, or web links for publicly available datasets
- A list of figures that have associated raw data
- A description of any restrictions on data availability

NGS data are publicly available (GSE93959)

Field-specific reporting

Please select the best fit for your research. If you are not sure, read the appropriate sections before making your selection.

Life sciences Behavioural & social sciences Ecological, evolutionary & environmental sciences

For a reference copy of the document with all sections, see nature.com/authors/policies/ReportingSummary-flat.pdf

Life sciences study design

All studies must disclose on these points even when the disclosure is negative.

Sample size	Samples sizes were determined by NGS data depth. The number of data points was more than sufficient to arrive at the drawn conclusions in a statistically significant manner (evidenced by p values). For molecular biology experiments, three or more independent replicates were measured, allowing the drawing of statistically significant conclusions (evidenced by p values).
Data exclusions	Data points representing low sequencing read numbers were excluded from analyses (customary for sequencing experiments). Cutoffs, where applicable, are noted for each experiment in Materials and Methods Section.
Replication	All experiments were performed in two or more biological replicates (described for each experiment in Materials and Methods Section)
Randomization	Randomization was not relevant to our study, since we did not deal with human or animal subjects.
Blinding	Randomization was not relevant to our study, since we did not deal with human or animal subjects.

Reporting for specific materials, systems and methods

Materials & experimental systems

n/a	Involved in the study
<input type="checkbox"/>	<input checked="" type="checkbox"/> Unique biological materials
<input type="checkbox"/>	<input checked="" type="checkbox"/> Antibodies
<input checked="" type="checkbox"/>	<input type="checkbox"/> Eukaryotic cell lines
<input checked="" type="checkbox"/>	<input type="checkbox"/> Palaeontology
<input checked="" type="checkbox"/>	<input type="checkbox"/> Animals and other organisms
<input checked="" type="checkbox"/>	<input type="checkbox"/> Human research participants

Methods

n/a	Involved in the study
<input checked="" type="checkbox"/>	<input type="checkbox"/> ChIP-seq
<input checked="" type="checkbox"/>	<input type="checkbox"/> Flow cytometry
<input checked="" type="checkbox"/>	<input type="checkbox"/> MRI-based neuroimaging

Unique biological materials

Policy information about [availability of materials](#)

Obtaining unique materials All unique materials are freely available from the authors.

Antibodies

Antibodies used

anti-Ded1p, anti-Hxk1p

Validation

anti-Ded1p is a polyclonal antibody raised against full length recombinant Ded1p. The Ab has been validated extensively against recombinant Ded1p and for specificity (e.g. refs.24,25). anti-Hxk1 antibody is a commercial antibody (U.S. Biological)